


Mutual amplification of high-order harmonics in an optically dressed hydrogenlike plasma-based x-ray laser

I. R. Khairulin ^{1,2,*}, V. A. Antonov,¹ M. Yu. Ryabikin,^{1,2} and Olga Kocharovskaya³

¹*Institute of Applied Physics of the Russian Academy of Sciences, 46 Ulyanov Street, Nizhny Novgorod 603950, Russia*

²*N. I. Lobachevsky State University of Nizhny Novgorod, 23 Gagarin Avenue, Nizhny Novgorod 603950, Russia*

³*Department of Physics and Astronomy and Institute for Quantum Studies and Engineering, Texas A&M University, College Station, Texas 77843, USA*



(Received 3 August 2022; accepted 19 January 2023; published 9 February 2023)

In a recent work [V. A. Antonov, K. C. Han, T. R. Akhmedzhanov, M. Scully, and O. Kocharovskaya, *Phys. Rev. Lett.* **123**, 243903 (2019)] a method of amplifying a train of attosecond pulses, produced via high-order harmonic generation of an infrared (IR) laser field, in an active medium of a plasma-based x-ray laser dressed by a replica of the IR field of the fundamental frequency was proposed. The specific case of independent amplification of each incident harmonic was considered, corresponding to a dense plasma of multiply charged ions (such as C^{5+} ions) which is strongly dispersive for the IR field. In the present paper, we consider a general case when the laser field modulation leads not only to the direct amplification of high harmonics (HHs), but also to the scattering of the harmonics into each other. The mutual coherent scattering process plays an important role in a relatively low-density plasma with a lower ion charge, corresponding to a weakly dispersive plasma at the frequency of the IR field. Constructive interference between the amplified HHs and the coherently scattered field may result in a significant enhancement of the total output field. We call this effect the mutual amplification of high-order harmonics. Considering the plasma of hydrogenlike Li^{2+} ions with an inverted transition wavelength of 13.5 nm as an example, we analytically and numerically show that synchronization of a coherently scattered field with the radiation of amplified HHs makes it possible to increase the intensity of attosecond pulses by several times compared to the case of an independent amplification of HHs.

DOI: [10.1103/PhysRevA.107.023507](https://doi.org/10.1103/PhysRevA.107.023507)

I. INTRODUCTION

At the end of the 20th and beginning of the 21st century a new interdisciplinary field of research, called attosecond physics, emerged and began to rapidly develop, which is aimed at investigating and controlling the ultrafast processes in atoms, molecules, and solids on their intrinsic time scales [1–7]. This became possible due to the development of the sources of attosecond extreme ultraviolet (XUV) and x-ray pulses based on high-order harmonic generation (HHG) of intense optical and infrared (IR) laser fields in gases in the tunnel ionization regime [8–10]. Nowadays, the pulses generated by such sources can be as short as 40–50 as [11–13]. However, the corresponding pulse energy in the x-ray range does not exceed a few nJ at best [14,15], mainly because of significant limitations on high-order harmonic yield due to the macroscopic pulse propagation effects [16]. This limits the practical applications of HHG sources, in particular, those related to the single-shot measurements of ultrafast processes in matter, as well as initiating and studying nonlinear processes in the XUV and x-ray range [17,18]. Thus, enhancing the energy of high harmonics (HHs) and attosecond pulses is an important task from both fundamental and practical points of view.

One may consider two ways to increase the energy of HHs. The first one is to optimize the conditions for generating HHs in order to enhance their yield. The resultant harmonic yield is determined by (i) a single-atom (microscopic) response, which characterizes the strength of interaction of each atom with the driving laser field during the three-step HHG process (ionization of an atom, acceleration of the free electron, and its recombination with the parent ion), and (ii) the macroscopic response associated with the coherent summation of HH emission from individual atoms. Enhancement of the macroscopic response can be achieved by creating the favorable phase-matching conditions, which can be done by adjusting the laser intensity, its wavelength, and focusing parameters, as well as the parameters of the gas [16,19–24]. The microscopic response can be enhanced by optimizing the ionization of the atom, as well as the electron dynamics in the driving laser field. It can be accomplished by (i) modifying the sub-laser-cycle waveform of the driving field via adding the low-order (second and/or third) harmonics to its fundamental frequency [25–31] and/or (ii) seeding the interaction medium with the radiation of a single HH or a set of HHs, forming a train of attosecond pulses [32–36]. In the latter case, it is possible to enhance the HH yield by two to four orders of magnitude, taking into account the macroscopic propagation effects.

The second way to increase the HH energy is to use an additional amplifier. In [37] it was theoretically proposed to amplify a train of attosecond pulses, produced via HHG in

*Corresponding author: khairulinir@ipfran.ru

a gas, in an x-ray free-electron laser (XFEL) in the mode locking regime [38], when a series of spatiotemporal shifts is introduced between the radiation and the copropagating electron bunch by delaying the electron bunch using magnetic chicanes inserted between undulator modules. In this case, the possibility of amplifying a train of attosecond pulses of widths ≈ 300 as with peak power up to 1 GW was theoretically shown. However, XFELs are large-scale and very expensive facilities, and there are very few of them available in the world. Another way is to use a laboratory-scale plasma-based x-ray laser for HH amplification. In this case, the energy of the seeding HH radiation pulse can be amplified up to $1 \mu\text{J}$ [39–41]. However, the narrow bandwidth (mÅ) of such amplifier [42,43] leads to accumulating the energy obtained in the amplification process in the radiation of a single HH resonant with the inverted transition of the active medium. This fact does not allow direct amplification of a set of HHs, and hence attosecond pulses, in such active media.

In the recent work [44], we proposed a method that allows one to broaden the gain spectrum of a plasma-based x-ray laser and to use it for the amplification of an attosecond pulse train formed by a set of HHs of an optical or IR laser field. For this purpose, an active medium of an x-ray laser should be irradiated by a replica of the fundamental frequency laser field (or its second harmonic [45]) used for generating the seeding HHs. Originally, this method was proposed for a hydrogenlike active plasma medium [44,45], and then generalized to the case of a neonlike active medium [46]. Under the action of the laser field due to the Stark effect (the linear Stark effect in the case of hydrogenlike ions and the quadratic Stark effect in the case of neonlike ions), the transition frequencies between the lasing states of the ions follow the local value of the electric field of the laser wave in time and space. Thus, the laser field produces a subcycle modulation of the medium. As a result, the medium gain, initially localized in the vicinity of the frequency of the inverted transition, is redistributed to the combination frequencies separated from the resonance (taking into account its time-averaged Stark shift) by multiples of the modulating field frequency in the case of a hydrogenlike medium or by even multiples of the modulating field frequency in the case of a neonlike medium. In this case, if one of the HHs of the modulating field is tuned in resonance with the time-averaged frequency of the inverted transition, then the other HHs will be automatically resonant with the corresponding induced gain lines. If, in addition, the plasma dispersion at the frequency of the modulating field is strong enough, then the harmonics of different orders will be amplified independently of each other, and their relative phases will be preserved. Such regime is realized in active media with high free-electron concentration, in particular, with population inversion at the transition of highly charged ions, for example, hydrogenlike C^{5+} ions [44,45] and neonlike Ti^{12+} ions [46]. Furthermore, the gain coefficients for harmonics of different orders can be made approximately equal to each other via the proper choice of intensity of the modulating field. In this case, the relative amplitudes of HHs are approximately preserved during their amplification. Thus, if HHs form a train of attosecond pulses at the entrance to the medium, then, during the propagation through the medium, the intensity of the pulses will grow, while maintaining their duration and

shape. In particular, in [44,45] we showed the possibility of amplifying the attosecond pulses by two orders of magnitude in intensity in the hydrogenlike active plasma medium of C^{5+} ions.

On the other hand, in an active medium with a relatively weak plasma dispersion at frequency of the modulating field, a quasimonochromatic seeding XUV radiation, in particular, a single HH, which is turned into resonance with any of the induced gain lines, is not only amplified, but also generates a coherently scattered field at the combination frequencies separated from the frequency of the seeding radiation by even multiples of the frequency of the modulating laser. Under the optimal conditions, the generated sidebands have comparable amplitudes and are in phase with the amplified seeding radiation, which leads to transformation of a quasimonochromatic seeding field (a single HH) into a train of subfemtosecond and attosecond pulses [47–50].

Moreover, as it was in [51], if there is a set of three HHs at the entrance to an active medium, then the interference of the amplified HHs with a multifrequency coherently scattered field opens up the possibility of controlling the power spectral density of HHs. As a result, the total energy of radiation of a set of three HHs can increase or decrease due to constructive or destructive interference with a coherently scattered field, and the asymmetry of the HH spectrum can be controlled. However, the optimal conditions under which the harmonic amplification efficiency is maximized have not been analyzed.

In the present paper, we consider the general case of amplification of high harmonics, when the scattering process needs to be taken into account. We study the possibility of increasing the efficiency of amplification of attosecond pulses formed by a set of (three, five, and seven) in-phase HHs in the modulated active medium of a plasma-based x-ray laser due to synchronization of the coherently scattered field with amplified HHs. Hereinafter, for brevity, we will call this effect mutual amplification of high-order harmonics (MAHH). Contrary to [51], we focus on the time dependence of the HH signal and the preservation of the duration and shape of the amplified pulses (which is nontrivial, since the interference of the HHs with a coherently scattered field generally changes the relative harmonic phases). We derive a more general, in comparison with [51], analytical solution for the field of HHs in an optically deep active plasma medium, which accounts for the rescattering of harmonics into each other and is valid for an arbitrary shape of the HH spectral line. Based on the obtained analytical solution, we find the optimal conditions for MAHH, under which the maximum increase in the intensity of the amplified pulses of high harmonics is achieved while maintaining their shape and duration, and confirm the results by numerical integration of the Maxwell-Bloch equations. As an active medium, we consider an active plasma of hydrogenlike Li^{2+} ions, as was done in [48,50,51].

The paper is organized as follows. In Sec. II we briefly present a theoretical model describing the HH amplification in a modulated hydrogenlike active plasma medium. In Sec. III we derive a generalized analytical solution, which allows one to better understand the main features of MAHH, and use it to find the optimal conditions for the mutual amplification of three (Sec. IIIA), five (Sec. IIIB), and seven (Sec. IIIC) in-phase HHs. In Sec. IV the results of the analytical theory

are compared with the results of the numerical solutions of the system of equations given in Sec. II. Finally, in Sec. V we summarize the main results of this paper.

II. BASIC CONCEPT

Below, we consider an amplification of a set of $(2N + 1)$ linearly polarized high-order harmonics of an IR laser field in an active medium of a recombination plasma-based x-ray laser, which consists of hydrogenlike ions and free electrons, with a population inversion at the transition $n = 1 \leftrightarrow n = 2$ of the ions (where n is the principal quantum number). XUV and x-ray lasing in such an active medium has been studied in a number of works [52,53]. The active medium is simultaneously irradiated by the copropagating IR field of the fundamental frequency with the same linear polarization:

$$\vec{E}_L(x, \tau) = \vec{z}_0 E_{\text{IR}} \cos(\Omega\tau + \Delta Kx + \vartheta), \quad (1)$$

where $\tau = t - x\sqrt{\varepsilon_{\text{XUV}}}/c$ is the local time in the reference frame, which moves along with the wavefront of the HH field; c is the speed of light in vacuum; $\varepsilon_{\text{XUV}} = 1 - 4\pi e^2 N_e / (m_e \omega_{\text{inc}}^2)$ is the nonresonant dielectric permittivity of the plasma for a set of HHs with the carrier frequency ω_{inc} ; the x axis is the propagation direction; the z axis is the polarization direction; \vec{z}_0 is the unit vector along the z axis; E_{IR} and Ω are, respectively, the amplitude and the angular frequency of the IR field; ϑ is its initial phase, which characterizes the sub-laser-cycle delay of HH pulses relative to the modulating field; $\Delta K = \Omega(\sqrt{\varepsilon_{\text{XUV}}} - n_{\text{pl}})/c$ is the difference between the wavenumbers of the IR field in the medium with the refractive index $\sqrt{\varepsilon_{\text{XUV}}}$ and in the plasma with electron concentration N_e ; $n_{\text{pl}} = \sqrt{1 - 4\pi e^2 N_e / (m_e \Omega^2)}$ is the plasma refractive index for the IR field; e and m_e are the electron charge and mass, respectively. Here we assume that (i) the transverse and longitudinal distributions of the IR field are much wider than, respectively, the cross section and the length of the plasma channel and (ii) the IR field pulse duration is quite large compared to the relaxation times of the medium. It is also assumed that the amplitude of the laser field is smaller than the ionization threshold from the excited (upper lasing) energy level of the ions, so that it does not additionally ionize the medium. Under the action of the IR field, the energy level with $n = 2$ splits into three sublevels. Two of them correspond to the states $|2\rangle = (|2s\rangle + |2p, m = 0\rangle)/\sqrt{2}$ and $|3\rangle = (|2s\rangle - |2p, m = 0\rangle)/\sqrt{2}$, which are the energy eigenstates of the hydrogenlike ions in parabolic coordinates with principal z axis. The energies of these states oscillate in space and time along with oscillation of the IR field strength (1) due to the linear Stark effect and also acquire a constant shift due to the quadratic Stark effect. The third sublevel is degenerate and corresponds to the states $|4\rangle = |2p, m = 1\rangle$ and $|5\rangle = |2p, m = -1\rangle$. These states experience only a quadratic Stark shift, which can be considered as space-time independent [54]. Thus, the frequencies of the transitions from the excited states of the ions $|i\rangle$ ($i = 2,3,4,5$) to the ground state

$|1\rangle = |1s\rangle$ take the form

$$\begin{aligned} \omega_{21}(\tau, x) &= \omega_z - \Delta\Omega \cos(\Omega\tau + \Delta Kx + \vartheta), \\ \omega_{31}(\tau, x) &= \omega_z + \Delta\Omega \cos(\Omega\tau + \Delta Kx + \vartheta), \\ \omega_{41} &= \omega_{51} = \omega_y, \end{aligned} \quad (2)$$

where $\omega_z = [\frac{3m_e e^4 Z^2}{(8\hbar^3)}](1 - \frac{109F_0^2}{64})$ and $\omega_y = [\frac{3m_e e^4 Z^2}{(8\hbar^3)}](1 - \frac{101F_0^2}{64})$ are the time-averaged frequencies of the transitions $|2\rangle \rightarrow |1\rangle$, $|3\rangle \rightarrow |1\rangle$ and $|4\rangle \rightarrow |1\rangle$, $|5\rangle \rightarrow |1\rangle$, respectively; $\Delta\Omega = 3m_e e^4 Z^2 F_0 / (8\hbar^3)$ is the amplitude of linear Stark shift; $F_0 = (2/Z)^3 E_{\text{IR}} / E_A$ is the normalized amplitude of the IR laser field; $E_A \simeq 5.14 \times 10^9 \frac{\text{V}}{\text{cm}}$ is the atomic unit of the electric field; Z is the charge number of the ions; \hbar is Planck's constant. Here the use of indices z and y is justified by the fact that the dipole moments of transitions $|2\rangle \rightarrow |1\rangle$, $|3\rangle \rightarrow |1\rangle$ are oriented along the z axis, while the dipole moments of transitions $|4\rangle \rightarrow |1\rangle$, $|5\rangle \rightarrow |1\rangle$ have components along the x and y axes; however, the field propagating along the x axis interacts only with their y components.

In the following, we assume that at the entrance to the medium there are $(2N + 1)$ high-order harmonics of the fundamental frequency Ω , which are in phase with each other, have the same amplitudes E_0 , and are polarized along the z axis [as the laser field (1)]. Thus, the HHs interact with the modulated transitions $|2\rangle \rightarrow |1\rangle$ and $|3\rangle \rightarrow |1\rangle$. In the time domain, they constitute a train of pulses with duration $T/(2N + 1)$ and repetition period $T/2$, where $T = 2\pi/\Omega$ is the IR field cycle. The electric field of the pulse train at the entrance to the medium has the form

$$\begin{aligned} \vec{E}(x = 0, \tau) &= \frac{1}{2} \vec{z}_0 E_{\text{in}}(\tau) \exp(-i\omega_{\text{inc}}\tau) \\ &\times \sum_{n=-N}^N \exp(-in2\Omega\tau) + \text{c.c.}, \end{aligned} \quad (3)$$

where $E_{\text{in}}(\tau)$ is its envelope. We assume that $E_{\text{in}}(\tau) = E_0\theta(\tau)$, where $\theta(\tau)$ is the Heaviside step function. As shown below, such a choice of the envelope of the pulse train allows obtaining the simple analytical solution to the considered problem. Further, we suppose that the carrier frequency of the HH field equals to the time-averaged frequency of the transitions $|2\rangle \rightarrow |1\rangle$ and $|3\rangle \rightarrow |1\rangle$, that is, $\omega_{\text{inc}} = \omega_z$, which results in their strongest amplification.

In turn, the transitions $|4\rangle \rightarrow |1\rangle$ and $|5\rangle \rightarrow |1\rangle$ lead to the generation of the y -polarized XUV or x-ray amplified spontaneous emission (ASE), which (i) reduces the gain for the z -polarized HH field by increasing the population of the ground state of the ions and (ii) overlaps in time with the amplified HH signal. The ASE can be suppressed by using a sufficiently strong seeding z -polarized HH field.

The amplification of the pulse train (3) can be described by the system of Maxwell-Bloch equations within the five-level model of the medium using the slowly varying amplitude approximation and the rotating wave approximation. This system of equations is presented in [44,47,48] and will not be reproduced here because of its large volume.

In the next section, we derive an analytical solution that describes the main features of the HH field (3) amplified in a

hydrogenlike active medium with moderate plasma dispersion for the modulating IR field.

III. ANALYTICAL THEORY

The analytical solution obtained below is based on the following approximations. We assume that the incident z -polarized field (3) is sufficiently strong, so that the HH field dominates over the ASE of y polarization at all considered propagation distances. In this case, one may neglect the states $|4\rangle$, $|5\rangle$ and describe the active medium within the three-level model taking into account only the states $|1\rangle$, $|2\rangle$, and $|3\rangle$. We also assume a constant population difference n_{tr} at the transitions $|2\rangle \rightarrow |1\rangle$ and $|3\rangle \rightarrow |1\rangle$ (under the conditions considered below, the population differences at these transitions are the same), which corresponds to the linear regime of the HH amplification. Then, within the slowly varying amplitude approximation and the rotating wave approximation, the system of Maxwell-Bloch equations is reduced to

$$\begin{aligned} \frac{\partial \tilde{E}_z}{\partial x} &= i \frac{4\pi\omega_z N_{\text{ion}} d_{\text{tr}}}{c\sqrt{\epsilon_{\text{XUV}}}} (\tilde{\rho}_{21} - \tilde{\rho}_{31}), \\ \frac{\partial \tilde{\rho}_{21}}{\partial \tau} &= [-\gamma_z + i\Delta_\Omega \cos(\Omega\tau + \Delta Kx + \vartheta)] \tilde{\rho}_{21} - i \frac{d_{\text{tr}} n_{\text{tr}}}{2\hbar} \tilde{E}_z, \\ \frac{\partial \tilde{\rho}_{31}}{\partial \tau} &= [-\gamma_z - i\Delta_\Omega \cos(\Omega\tau + \Delta Kx + \vartheta)] \tilde{\rho}_{31} + i \frac{d_{\text{tr}} n_{\text{tr}}}{2\hbar} \tilde{E}_z, \end{aligned} \quad (4)$$

where \tilde{E}_z and $\tilde{\rho}_{i1}$, $i = 2, 3$, are the slowly varying amplitudes of the electric field of HHs and the quantum coherencies at the transitions $|2\rangle \rightarrow |1\rangle$ and $|3\rangle \rightarrow |1\rangle$, respectively. The latter determine the slowly varying amplitude of the resonant polarization of the medium, $\tilde{P}_z = N_{\text{ion}} d_{\text{tr}} (\tilde{\rho}_{21} - \tilde{\rho}_{31})$, where N_{ion} is the concentration of the resonant ions, $d_{\text{tr}} = (2^7/3^5)ea_0/Z$ is the dipole moment of the transitions $|2\rangle \rightarrow |1\rangle$ and $|3\rangle \rightarrow |1\rangle$, and a_0 is Bohr's radius. $\gamma_z = \gamma_z^{(0)} + \Gamma_{\text{ion}}/2$ is the relaxation rate of the quantum coherencies at these transitions; $\gamma_z^{(0)} = \gamma_{\text{coll}} + \Gamma_{\text{rad}}/2$ is the decoherence rate in the absence of the IR field; γ_{coll} and $\Gamma_{\text{rad}}/2$ are the collisional and radiative decay rates of the quantum coherencies at the inverted transitions in the absence of the IR field, respectively; $\Gamma_{\text{ion}} = \frac{m_e e^4 Z^2}{16\hbar^3} \sqrt{\frac{3F_0}{\pi}} \left[\frac{4}{F_0} e^3 + \left(\frac{4}{F_0}\right)^3 e^{-3} \right] e^{-\frac{2}{3F_0}}$ is the tunnel ionization rate from the states $|2\rangle$ and $|3\rangle$ under the action of the IR field averaged over the period of the modulating field. It is worth noting that apart from the Stark effect, the modulating field should lead not only to the tunnel ionization from the excited states, but also to the plasma heating, thus changing the value of γ_{coll} . As can be seen from the analytical solution obtained below, this should only lead to (i) a change in the medium gain and (ii) a change in the response time of the resonant polarization of the medium. However, in what follows, we will neglect this change in γ_{coll} , since a quantitative description of this effect is beyond the scope of this paper.

We seek a solution for \tilde{E}_z in the form

$$\tilde{E}_z(x, \tau) = \int_{-\infty}^{\infty} \sum_{n=-N}^N \tilde{A}_n(x, \omega - 2n\Omega) e^{-i\omega\tau} d\omega, \quad (5)$$

where $\tilde{A}_n(\omega)$ is the spectral amplitude of the n th harmonic (for simplicity, we will call the harmonic at the frequency

$\omega_{\text{inc}} + 2n\Omega$ “ n th harmonic”). Equation (5) implies that the spectral composition of the HH field in the medium is determined by the radiation of the seed (3) (no new sidebands are generated in the spectrum of HHs). In the following, we will additionally assume that (i) the spectral contours of the harmonics of different orders do not overlap with each other and (ii) the spectral separation between the harmonics is much larger than the gain bandwidth of the active medium, $\Omega \gg \gamma_z$. In this case, as shown in Appendix A, the system of Eqs. (4) for the spectral amplitudes of the HHs, $\tilde{A}_n(\omega)$, can be reduced to the system of the interrelated equations:

$$\begin{aligned} \tilde{A}_n(x, \omega) &= \tilde{A}_n(x=0, \omega) e^{g_{nm}x/(1-i\omega/\gamma_z)} \\ &+ \sum_{\substack{m=-N \\ m \neq n}}^N \frac{g_{nm} e^{i2(m-n)\vartheta}}{1-i\omega/\gamma_z} \int_0^x \tilde{A}_m(x', \omega) \\ &\times e^{g_{mn}(x-x')/(1-i\omega/\gamma_z) + i2(m-n)\Delta Kx'} dx', \end{aligned} \quad (6)$$

where $g_{nm} = g_0 J_{2n}(P_\Omega) J_{2m}(P_\Omega)$ is the coefficient of coherent scattering of the m th harmonic into the n th harmonic, while g_{mn} is the effective gain coefficient of the n th harmonic in a dense plasma medium; $g_0 = 4\pi\omega_z d_{\text{tr}}^2 n_{\text{tr}} N_{\text{ion}} / (\hbar c \sqrt{\epsilon_{\text{XUV}}} \gamma_z)$ is the amplitude gain factor of resonant radiation in the absence of modulation; $J_m(x)$ is the Bessel function of the first kind of order m ; $P_\Omega = \Delta_\Omega/\Omega$ is the modulation index, which is the amplitude of the linear Stark shift (the normalized amplitude of the IR field, E_{IR}) divided by the frequency of the IR field, Ω ; while $\tilde{A}_n(x=0, \omega)$ is the spectral amplitude of the n th HH at the entrance to the medium. In accordance with (3), all HHs at $x=0$ have identical spectral amplitudes: $\tilde{A}_n(x=0, \omega) = \tilde{A}_0(\omega) = \frac{1}{2\pi} \int_{-\infty}^{\infty} E_{\text{in}}(\tau) e^{i\omega\tau} d\tau$. The first term in (6) describes the amplification of the n th harmonic with the gain coefficient g_{nm} during its solitary propagation through the modulated active medium. The second term in (6) describes the influence of all other harmonics on the amplitude of the n th harmonic. Both the effective gain coefficients g_{nm} and the scattering coefficients g_{mn} depend on the amplitude and the frequency (wavelength) of the modulating field through the modulation index. Thus, the modulation index determines both the relative amplitudes of the gain coefficients for the harmonics of different orders and the efficiency of their mutual scattering. Note that the coefficients g_{nm} determine the efficiency of harmonic scattering into each other in a nondispersive active medium (with zero plasma dispersion for the modulating IR field), while the role of the plasma dispersion is taken into account by the integrals on the right-hand side of (6). The factor $(1-i\omega/\gamma_z)^{-1}$ both in the exponent and under the sum symbol in (6) characterizes the spectral contour of the gain lines, and it is responsible for modifying the shape of the spectral contours of HHs.

After normalizing the integration variable, Eqs. (6) can be represented as

$$\begin{aligned} \tilde{A}_n(x, \omega) &= \tilde{A}_0(\omega) e^{g_{nm}x/(1-i\omega/\gamma_z)} \\ &+ \sum_{\substack{m=-N \\ m \neq n}}^N \frac{g_{nm}}{\Delta K} \frac{e^{i2(m-n)\vartheta}}{1-i\omega/\gamma_z} \int_0^{\Delta Kx} \\ &\times \tilde{A}_m(\Phi/\Delta K, \omega) e^{\frac{g_{mn}}{\Delta K} (\Delta Kx - \Phi)/(1-i\omega/\gamma_z) + i2(m-n)\Phi} \\ &\times d\Phi, \end{aligned} \quad (7)$$

where $\Phi = \Delta K x'$ is the phase accumulated by the modulating IR field due to the plasma dispersion at the propagation distance x' . Let us introduce the parameter

$$\alpha = \frac{g_0}{\Delta K}, \quad (8)$$

which is the ratio between the amplitude gain coefficient of the nonmodulated medium, g_0 , and the addition to the wave number of the IR field caused by the plasma dispersion, ΔK .

If the plasma is strongly dispersive for the modulating IR field, and the parameter α tends to zero, $\alpha \rightarrow 0$, then the second term in (7) becomes negligible. In this case, each harmonic is amplified independently of the others with a gain coefficient proportional to $J_{2n}^2(P_\Omega)$, while the relative phases of the harmonics are maintained during the amplification process [44]. This can be understood as redistribution of medium gain to combination frequencies resonant with the HHs. If additionally the modulation index, P_Ω , is chosen in such a way that the squares of Bessel functions of different orders, $J_{2n}^2(P_\Omega)$, $n = 1, 2, \dots, N$, are maximized and have approximately the same values, then the harmonics resonant with the corresponding gain lines will be amplified uniformly (equally efficiently), and the time dependence of the resulting HH field will not be noticeably modified. In particular, this allows for the amplification of attosecond pulses with preservation of their duration and shape.

At the same time, as was shown in [47–50], in an active medium with low concentration of free electrons and moderate dispersion for the modulating IR field, a single HH, tuned in resonance with the modulated transition, efficiently generates a multifrequency XUV or x-ray field at the frequencies of the sidebands, separated from the resonance by even multiples of the frequency of the modulating field. This multifrequency field is generated due to the coherent scattering of the resonant radiation on the modulation wave, which propagates through the medium with the phase velocity of the modulating field. At the optimal depth of the medium, determined by the concentration of free electrons in a plasma, and for certain values of the modulation index, the sidebands acquire the highest amplitudes and become phase aligned with the amplified field of the resonant harmonic, which allows for the formation of subfemtosecond pulses from the quasimonochromatic incident radiation.

Contrary to [47–50], in the present paper we consider the propagation of an attosecond pulse train constituted by a set of $(2N + 1)$ in-phase harmonics, which are tuned in resonance with the induced gain lines, through the active plasma medium with low concentration of free electrons. In this case, each harmonic from the incident field is both amplified and generates coherently scattered fields at the frequencies of the other harmonics. A sum of these coherently scattered fields at the frequency of an individual harmonic forms the second term in (7). A single term in this sum characterizes the scattering of the field of the m th harmonic with the amplitude \tilde{E}_m to the field of the n th harmonic with the amplitude \tilde{E}_n . The efficiency of this scattering is proportional to the ratio $g_{nm}/\Delta K$. Thus, to increase the efficiency of mutual harmonic scattering, one needs to increase g_{nm} via increasing the unperturbed gain coefficient, g_0 , and maximizing the product $J_{2n}(P_\Omega)J_{2m}(P_\Omega)$,

and decrease the plasma dispersion at the frequency of the modulating field, thus decreasing ΔK .

It is worth noting that the efficiency of harmonic scattering into each other decreases with increasing harmonic detuning from the resonance (increasing absolute values of the indices $2n$ and $2m$). Indeed, the peak (with respect to variation of the modulation index) value of the product $J_{2n}(P_\Omega)J_{2m}(P_\Omega)$ decreases with increasing indices n and m . Moreover, with increasing n and m , the maximization of $J_{2n}(P_\Omega)J_{2m}(P_\Omega)$ implies a larger value of the modulation index $P_\Omega \geq \max(2|n|, 2|m|)$, where $P_\Omega \sim E_{\text{IR}}/\Omega \sim E_{\text{IR}}\Lambda$ (Λ is the wavelength of the modulating field). However, the value of P_Ω is limited for the following reasons. An increase in the IR field strength above the ionization threshold of the active medium would destroy the gain (thus reducing g_0), while an increase in the IR field wavelength would lead to an increase in the plasma dispersion for the modulating field (increasing ΔK).

Furthermore, the amplitude of the coherently scattered field of the m th harmonic at the frequency of the n th harmonic depends on the propagation distance through the parameter $\Delta K x$. This is due to the fact that such a field is the sum of partial waves generated in all the preceding slices of the medium via the scattering of the m th harmonic field on the modulation wave propagating with the phase velocity of the modulating field, which differs from the phase velocity of harmonics because of the plasma dispersion. As follows from (7), the amplitude of the m th harmonic also depends on the initial phase of the modulating field, ϑ . If the relation between ϑ and $\Delta K x$ is that the overall coherently scattered field [the second term in (7)] is in phase with the field of the amplified harmonic [the first term in (7)], then their constructive interference will enhance the harmonic amplification efficiency. This is the effect of MAHH.

Thus, for the most efficient amplification of a set of in-phase harmonics in a moderately dispersive for the IR field plasma medium, two conditions should be satisfied. First, one should equalize and maximize the gain coefficients for the harmonics of different orders, g_{nm} , and the scattering coefficients between them, g_{nm} , via a proper choice of the modulation index, which should be on the order of or higher than the number of the amplified harmonics, $P_\Omega \geq 2N$; see [44,45] for the details. In such a case

$$\begin{aligned} |J_{-2N}(P_\Omega)| &\approx |J_{-2N+2}(P_\Omega)| \approx \dots \approx |J_{2N-2}(P_\Omega)| \approx |J_{2N}(P_\Omega)| \\ &\equiv J(P_\Omega), \end{aligned} \quad (9)$$

where $J(P_\Omega)$ is the average value of $|J_{2n}(P_\Omega)|$ for $-N \leq n \leq N$ at the corresponding value of the modulation index, $J(P_\Omega) = \sum_{n=-N}^N |J_{2n}(P_\Omega)| / (2N + 1)$. Equation (9) is just the optimal condition for independent harmonic amplification in a strongly dispersive plasma medium [44]. The second condition is the maximization of MAHH via a proper choice of the medium length and the initial phase of the modulating IR field.

Let us assume that the condition (9) is satisfied via a proper choice of the modulation index P_Ω , while the parameter α is sufficiently small, so that the second term in (7) can be considered as a small perturbation. In this case, in the zeroth order of the perturbation theory the following equality holds: $\tilde{A}_n(x, \omega) = \tilde{A}_0(\omega) \exp[g_{\text{eff}}x / (1 - i\omega/\gamma_z)]$ for any

$-N \leq n \leq N$, where $g_{\text{eff}} = g_0 J^2(P_\Omega)$ is the effective gain coefficient. In the first order of the perturbation theory

$$\begin{aligned} \tilde{A}_n(x, \omega) = & \tilde{A}_0(\omega) e^{g_{\text{eff}} x / (1 - i\omega/\gamma_z)} \\ & \times \left[1 + \frac{\alpha J^2(P_\Omega)}{1 - i\omega/\gamma_z} \sum_{\substack{m=-N \\ m \neq n}}^N \text{sgn}[J_{2n} J_{2m}] \right. \\ & \left. \times \frac{\sin[(m-n)\Delta Kx]}{m-n} e^{i(m-n)(\Delta Kx + 2\vartheta)} \right], \end{aligned} \quad (10)$$

where $J_{2n} \equiv J_{2n}(P_\Omega)$ and $\text{sgn}(x) = 1$ for $x \geq 0$, $\text{sgn}(x) = -1$ for $x < 0$.

Let us formulate a sufficient condition for the applicability of the perturbation theory in this case. First, we estimate $J^2(P_\Omega)$. As was shown in [45], the gain spectrum of the optically dressed hydrogenlike active medium consists of the gain lines, which are separated from the resonance by both even and odd multiples of Ω with the peak gain coefficients proportional to $J_{2n}^2(P_\Omega)$ and $J_{2n+1}^2(P_\Omega)$, respectively. As is well known, $\sum_{n=-\infty}^{\infty} J_n^2(P_\Omega) = 1$. Under the condition (9) the total medium gain is redistributed approximately equally between the gain lines and one may assume $J_n^2(P_\Omega) \approx J_m^2(P_\Omega)$ for arbitrary n and m . For the most efficient amplification of the incident field (3), the number of even-order induced gain lines should be approximately equal to the number of amplified harmonics [44,45] (while the total number of the gain lines should be twice as large). Then $J^2(P_\Omega)$ can be estimated as $1/[2(2N+1)]$. Second, we estimate the sum in the second term in square brackets of (10). Since the absolute value of a sum is less than the sum of the absolute values of its terms and $|\sin(x)| \leq 1$, we can write

$$\begin{aligned} & \left| \sum_{\substack{m=-N \\ m \neq n}}^N \text{sgn}(J_{2n} J_{2m}) \frac{\sin[(m-n)\Delta Kx]}{m-n} e^{i(m-n)(\Delta Kx + 2\vartheta)} \right| \\ & \leq \sum_{\substack{m=-N \\ m \neq n}}^N \frac{1}{|m-n|}. \end{aligned} \quad (11)$$

By introducing the substitution $k = m - n$, we obtain

$$\sum_{\substack{k=-N-n \\ k \neq 0}}^{N-n} \frac{1}{|k|} = \sum_{k=1}^{N-n} \frac{1}{k} + \sum_{k=1}^{N+n} \frac{1}{k} \leq 2 \sum_{k=1}^N \frac{1}{k}. \quad (12)$$

The last sum in (12) is the partial sum of the harmonic series. It can be estimated as $\sum_{k=1}^N \frac{1}{k} \leq \ln(N) + 1$. Finally, $|1 - i\omega/\gamma_z|^{-1} \leq 1$. Thus, the sufficient condition for the applicability of perturbation theory takes the form

$$\alpha(\ln N + 1)/(2N + 1) \ll 1. \quad (13)$$

The condition (13) implies either (i) a relatively strong plasma dispersion for the modulating IR field, (ii) a not too large gain of an active medium for the XUV or x-ray field, or (iii) a high number of the amplified HHs.

The time dependence of the amplitude of the n th HH is calculated from (10) using the inverse Fourier transform and

has the form

$$\begin{aligned} \tilde{E}_n(x, \tau) = & \tilde{E}_{\text{indep}}(x, \tau) + \alpha J^2(P_\Omega) B(x, \tau) \\ & \times \sum_{\substack{m=-N \\ m \neq n}}^N \text{sgn}[J_{2n} J_{2m}] \frac{\sin[(m-n)\Delta Kx]}{m-n} \\ & \times e^{i(m-n)(\Delta Kx + 2\vartheta)}, \end{aligned} \quad (14)$$

where $\tilde{E}_{\text{indep}}(x, \tau) = \int_{-\infty}^{\infty} \tilde{A}_0(\omega) \exp[g_{\text{eff}} x / (1 - i\omega/\gamma_z)] e^{-i\omega\tau} d\omega$ is the spatial-temporal dependence of the amplitude of the n th HH in the case of its independent amplification in the modulated active medium, and $B(x, \tau) = \partial \tilde{E}_{\text{indep}}(x, \tau) / \partial (g_{\text{eff}} x)$ is a factor describing the space-time dependence of the coherently scattered field due to the fact that it is produced with a delay relative to the field of harmonics. As shown in Appendix B, for the considered envelope of the incident harmonic signal, $E_{\text{in}}(\tau) = E_0 \theta(\tau)$, $\tilde{E}_{\text{indep}}(x, \tau)$ has the following form:

$$\begin{aligned} \tilde{E}_{\text{indep}}(x, \tau) \\ = E_0 \theta(\tau) \left[1 + e^{-\gamma_z \tau} \sum_{k=0}^{\infty} \frac{(g_{\text{eff}} x)^{k+1}}{(k+1)!} \sum_{m=k+1}^{\infty} \frac{(\gamma_z \tau)^m}{m!} \right]. \end{aligned} \quad (15)$$

At the initial times, when $\gamma_z \tau < 1$, $\tilde{E}_{\text{indep}}(x, \tau)$ is approximately described by the following expression [see (B10) in Appendix B]: $\tilde{E}_{\text{indep}}(x, \tau) \simeq E_0 \theta(\tau) [1 + e^{-\gamma_z \tau} (I_0(2\sqrt{g_{\text{eff}} x \gamma_z \tau}) - 1)]$, where $I_0(x)$ is the modified zeroth-order Bessel function.

According to (14), the amplitude of the contribution due to the scattering of the m th harmonic into the n th harmonic [each term in the sum in (14)] is determined by the phase accumulated by the modulating field, ΔKx , as well as the difference $m - n$ and the derivative of the HH amplitude in the case of its independent amplification with respect to the effective optical thickness, $g_{\text{eff}} x$, of the modulated active medium, while the phase of this contribution is the function of the combination $\Delta Kx + 2\vartheta$, the sign of the product of the Bessel functions $J_{2n}(P_\Omega)$ and $J_{2m}(P_\Omega)$, and the sign of $\sin[(m-n)\Delta Kx]/(m-n)$. For a fixed initial phase of the modulating field, ϑ , the total coherently scattered field at the frequency of the n th harmonic is a quasiperiodic function of the propagation distance with the period $L_p = \pi/\Delta K$, while for a fixed propagation distance, x , it is a periodic function of ϑ with the period $\vartheta_p = \pi$. At the propagation distances corresponding to $\Delta Kx = k\pi$, where k is an integer, the coherently scattered field becomes zero and the harmonic amplitudes are the same as in the dense plasma medium. Although the analytical solution (14) implies the fulfillment of the condition (13), as shown below in Sec. IV via comparison with the numerical solution of the general system of equations described in Sec. II, it remains qualitatively correct even if the condition (13) is not satisfied.

The MAHH effect is observed if the sum in (14) is positive for each of the amplified HHs. To study the role of mutual scattering of in-phase HHs, forming a train of short pulses, in

their amplification process, we introduce the parameter

$$G_{\text{coh}}(x, \tau, P_{\Omega}, \vartheta) = \frac{I_{\text{pulse}} - I_{\text{pulse}}^{(\text{indep})}}{I_{\text{pulse}}^{(\text{indep})}}. \quad (16)$$

Here I_{pulse} is the peak intensity of an individual pulse in the amplified pulse train in the presence of MAHH, $I_{\text{pulse}} = \max[\frac{c}{8\pi} |\sum_{n=-N}^N \tilde{E}_n(x, \tau) e^{-i2n\Omega\tau}|^2]$, where the maximum is taken within the half cycle of the IR field in the vicinity of the time τ , while $I_{\text{pulse}}^{(\text{indep})}$ is the same value in the absence of the mutual harmonic scattering. $G_{\text{coh}} > 0$, if the overall contribution of the coherently scattered field to the harmonic intensity is positive, and $G_{\text{coh}} \leq 0$ otherwise. In the case of $G_{\text{coh}} < 0$ the harmonic amplification is suppressed because of the destructive interference of coherently scattered fields with the fields of HHs [51].

Under conditions of uniform harmonic amplification (9) we have $I_{\text{pulse}}^{(\text{indep})} = (2N + 1)^2 \max[c\tilde{E}_{\text{indep}}^2(x, \tau)/(8\pi)]$, while in the case of weak harmonic scattering (13), up to the first-order values in amplitude of the coherently scattered field, the parameter G_{coh} takes the form

$$G_{\text{coh}}(x, \tau, P_{\Omega}, \vartheta) = 2\alpha f(x, \tau) J^2(P_{\Omega}) F_{\text{interf}}(\Delta Kx, \vartheta, P_{\Omega}), \quad (17)$$

where $f(x, \tau) = B(x, \tau)/\tilde{E}_{\text{indep}}(x, \tau)$ and

$$\begin{aligned} F_{\text{interf}}(\Delta Kx, \vartheta, P_{\Omega}) &= \frac{1}{2N + 1} \sum_{n=-N}^N \sum_{\substack{m=-N \\ m \neq n}}^N \text{sgn}(J_{2n} J_{2m}) \\ &\times \frac{\sin[(m-n)\Delta Kx]}{m-n} \cos[(m-n)(\Delta Kx + 2\vartheta)]. \end{aligned} \quad (18)$$

The time dependence of the parameter G_{coh} is determined by the ratio between the electric-field amplitude of an amplified HH at the considered propagation distance x in the case of its independent amplification (in a dense active plasma medium), $\tilde{E}_{\text{indep}}(x, \tau)$, and the factor $B(x, \tau)$ [see Eq. (14) and the following discussion]. For the considered envelope of the incident harmonic signal (3) it has the form

$$f(x, \tau) = \frac{e^{-\gamma_z \tau} \sum_{k=0}^{\infty} \frac{(g_{\text{eff}} x)^k}{k!} \sum_{m=k+1}^{\infty} \frac{(\gamma_z \tau)^m}{m!}}{1 + e^{-\gamma_z \tau} \sum_{k=0}^{\infty} \frac{(g_{\text{eff}} x)^{k+1}}{(k+1)!} \sum_{m=k+1}^{\infty} \frac{(\gamma_z \tau)^m}{m!}}. \quad (19)$$

The time dependences of the factor f given by (19) for different values of the effective optical thickness, $g_{\text{eff}} x$, are shown in Fig. 1. According to this figure, the value of f increases monotonically with time and reaches saturation, $f \simeq 1$, at $\gamma_z \tau \gg 1$. In an optically thin medium, if $g_{\text{eff}} x \ll 1$, the factor f does not depend on the propagation distance and approximately equals to $f(x, \tau) \approx 1 - \exp(-\gamma_z \tau)$. In this case, the saturation time of the dependence $f(x, \tau)$ is given by the inverse decoherence rate at the resonant transitions, γ_z^{-1} . However, as the optical thickness increases, the saturation time increases as well, which leads to a decrease in the value of f (and, hence, G_{coh}) at a fixed time τ (until the population differences at the transitions $|2\rangle \rightarrow |1\rangle$ and $|3\rangle \rightarrow |1\rangle$ do not decrease much, and the obtained analytical solution remains applicable). Thus, the factor $f(x, \tau)$ leads to (i) monotonic increase in G_{coh} with time and (ii) monotonic decrease in

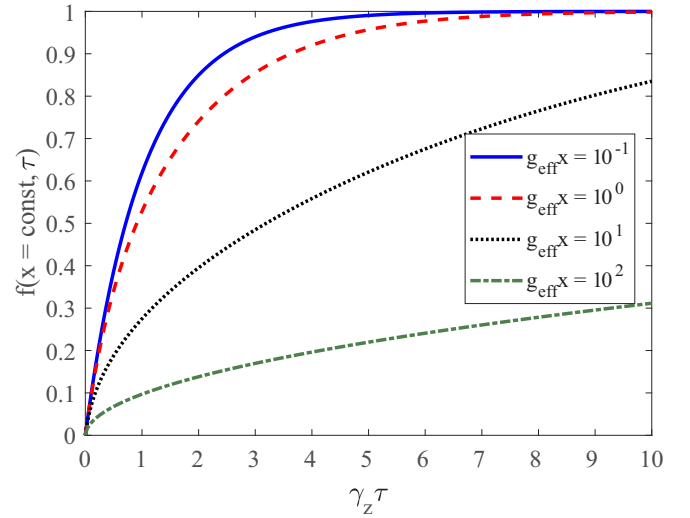


FIG. 1. The local time dependence of the factor f for different values of the effective optical thickness: $g_{\text{eff}} x = 10^{-1}$ (blue solid curve), $g_{\text{eff}} x = 10^0$ (red dashed curve), $g_{\text{eff}} x = 10^1$ (black dotted curve), and $g_{\text{eff}} x = 10^2$ (green dash-dotted curve).

G_{coh} with increasing effective optical thickness of the medium (increasing propagation distance).

Noteworthy, G_{coh} as a function of dimensionless parameters $\gamma_z \tau$, ΔKx , ϑ , and P_{Ω} does not depend on the characteristics of the active medium, except for the ratio $\alpha = g_0/\Delta K$.

In the next three subsections, we study the dependence of G_{coh} on the parameters ΔKx and ϑ at the values of P_{Ω} satisfying the condition (9) and find the optimal conditions, which maximize the value of G_{coh} , for the cases of mutual amplification of three, five, and seven in-phase HHs. For this purpose, the parameter G_{coh} is normalized to the factor $2\alpha f(g_{\text{eff}} x, \gamma_z \tau)$. This normalization allows one to obtain the results valid for arbitrary values of the parameters α , $g_{\text{eff}} x$, and $\gamma_z \tau$ within the range of applicability of the solution (14).

A. Mutual amplification of three in-phase HHs

We start with the case of a set of three HHs ($N = 1$). To find optimal conditions of their mutual amplification, it is necessary to maximize G_{coh} by finding the optimal values of the modulation index, P_{Ω} , the normalized propagation distance, ΔKx , and the initial phase of the modulating field, ϑ . For uniform amplification of all considered harmonics, the modulation index P_{Ω} should satisfy the condition (9). In the case of three HHs it is reduced to the following equation:

$$|J_0(P_{\Omega})| = |J_2(P_{\Omega})|. \quad (20)$$

The modulation indices satisfying (20) are

$$P_{\Omega} = \{1.84; 3.83; 5.33; 7.01; \dots\}. \quad (21)$$

In Fig. 2(a) we plot the dependencies $|J_0(P_{\Omega})|$ and $|J_2(P_{\Omega})|$, while in Fig. 2(b) we show $J^2(P_{\Omega})$ for modulation indices given by (21). The modulation indices (21) can be divided into two groups. The first group corresponds to those P_{Ω} , for which $J_0(P_{\Omega}) = J_2(P_{\Omega})$, while for modulation indices from the second group $J_0(P_{\Omega}) = -J_2(P_{\Omega})$. Such a difference leads

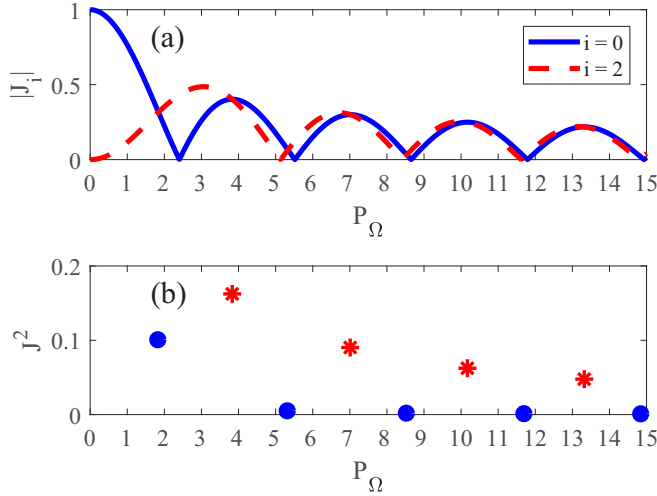


FIG. 2. (a) The modulation index dependence of the absolute value of the i th Bessel function. Blue solid and red dashed curves correspond to $i = 0$ and 2, respectively. (b) The square of the averaged absolute values of Bessel functions of orders $i = -2, 0, 2$ [denoted as $J^2(P_\Omega)$, see (9)] for the modulation indices satisfying (20). Blue circles correspond to the first group of P_Ω , for which $J_0(P_\Omega) = J_2(P_\Omega)$, and red stars correspond to the second group of P_Ω , for which $J_0(P_\Omega) = -J_2(P_\Omega)$.

to the different dependencies of F_{interf} on ΔKx and ϑ for these two groups.

Let us consider the first group of modulation indices. The corresponding dependence $F_{\text{interf}}^{(1)}(\Delta Kx, \vartheta)$ is shown in Fig. 3(a) (the superscript of the F_{interf} function indicates that the modulation index belongs to the first group). This dependence is plotted in the ranges $0 \leq \Delta Kx \leq \pi$ and $0 \leq \vartheta \leq \pi$ (due to the periodicity of F_{interf} , see Eq. (18), this is sufficient for its complete representation). It is worth noting that a change in ϑ by π does not lead to a physically different result, but an increase in the parameter ΔKx by π leads to a change in the physical thickness of the medium,

and, hence, to an increase in its effective optical thickness, as well as to a change in I_{pulse} and G_{coh} . The dependence $F_{\text{interf}}^{(1)}(\Delta Kx, \vartheta)$ contains several areas where $F_{\text{interf}} > 0$ (and thus $G_{\text{coh}} > 0$), and the total intensity of a set of HHs is higher than in the case of their independent amplification at the same physical length. Such areas contain the absolute maxima, $\max\{F_{\text{interf}}^{(1)}\} \simeq 1.47$, which are reached at $\Delta Kx \simeq 0.38\pi + p\pi$, where $p = \{0, 1, 2, \dots\}$, and $\vartheta \simeq 0.81\pi$. These maxima correspond to $\Delta Kx + 2\vartheta = 2\pi + p\pi$. In such a case, all the terms in (18) with $m-n = \{-2, -1, 0, 1, 2\}$ have the same (positive) signs. Consequently, the coherently scattered field (i) is maximized and (ii) is phase matched with the field of the amplified HHs.

Next, let us consider the second group of the modulation indices. In Fig. 3(b) we show the corresponding dependence $F_{\text{interf}}^{(2)}(\Delta Kx, \vartheta)$. It is clearly seen that Figs. 3(a) and 3(b) coincide up to a shift of ϑ by $\pi/2$. The reason is that such initial phase shift causes the appearance of a multiplier $(-1)^{m-n}$ in each term in (18), which is eliminated in the considered case of $N = 1$ (a set of three HHs) and $J_0(P_\Omega) = -J_2(P_\Omega)$ (the second group of the modulation indices), since $\text{sgn}(J_{2n}J_{2m}) = (-1)^{m-n}$. Thus, for such modulation indices the maxima of $F_{\text{interf}}^{(2)}(\Delta Kx, \vartheta)$, $\max\{F_{\text{interf}}^{(2)}\} = \max\{F_{\text{interf}}^{(1)}\} \simeq 1.47$, are reached at $\Delta Kx \simeq 0.38\pi + p\pi$, where $p = \{0, 1, 2, \dots\}$, and $\vartheta \simeq 0.31\pi$ (so that $\Delta Kx + 2\vartheta = \pi + p\pi$).

Now we can formulate the optimal conditions for MAHH for a set of three HHs, which maximize the parameter G_{coh} by maximizing the values of J^2 and F_{interf} . According to Figs. 2(b) and 3(b), the maxima are reached at $P_\Omega \equiv P_\Omega^{(3\text{Harm})} = 3.83$, $\Delta Kx \equiv (\Delta Kx)_{3\text{Harm}} \simeq 0.38\pi + p\pi$, where $p = \{0, 1, 2, \dots\}$, and $\vartheta \equiv \vartheta_{3\text{Harm}} \simeq 0.31\pi$. The corresponding peak value of G_{coh} normalized to the factor $2\alpha f(g_{\text{eff}x}, \gamma_z \tau)$ is about 0.24.

B. Mutual amplification of five in-phase HHs

Next, similar to the previous subsection, we consider the amplification of five in-phase HHs ($N = 2$). In this case,

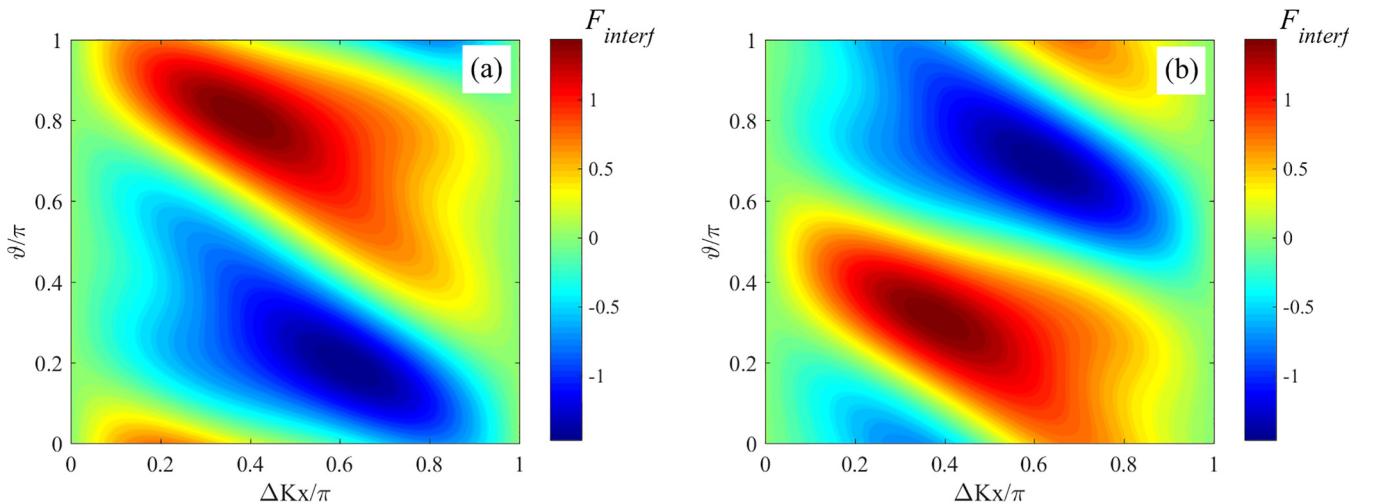


FIG. 3. The dependence of F_{interf} on the normalized propagation distance, ΔKx , and the initial phase of the modulating field, ϑ , for (a) the first group [blue circles in Fig. 2(b)] and (b) the second group [red stars in Fig. 2(b)] of the modulation indices, P_Ω .

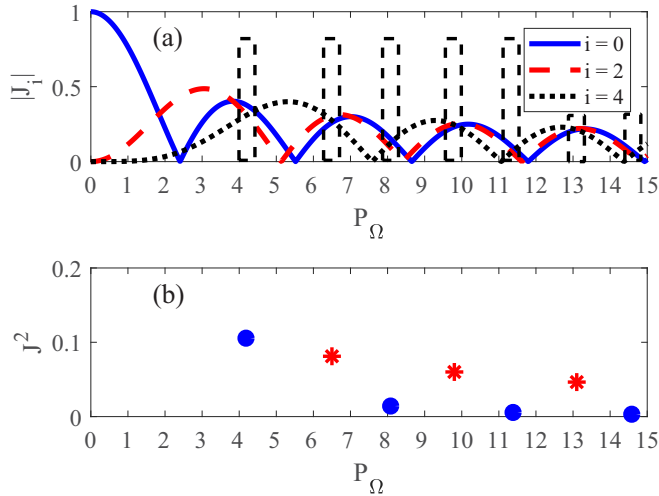


FIG. 4. (a) The modulation index dependence of the absolute value of the i th Bessel function. Blue solid, red dashed, and black dotted curves correspond to $i = 0, 2, 4$, respectively. Dashed black rectangles show the ranges of P_Ω , where the condition (22) is approximately satisfied. (b) The square of the averaged absolute values of Bessel functions of orders $i = -4, -2, 0, 2, 4$, $J^2(P_\Omega)$, for the modulation indices satisfying the condition (22). Blue circles correspond to the first group of P_Ω , for which $J_0(P_\Omega) \approx -J_2(P_\Omega) \approx -J_4(P_\Omega)$, and red stars correspond to the second group of P_Ω , for which $J_0(P_\Omega) \approx -J_2(P_\Omega) \approx J_4(P_\Omega)$.

the optimal value of the modulation index should satisfy the condition

$$|J_0(P_\Omega)| \simeq |J_2(P_\Omega)| \simeq |J_4(P_\Omega)|. \quad (22)$$

In Fig. 4(a) we plot the dependences of absolute values of Bessel functions of the zeroth, second, and fourth orders on the modulation index. According to this figure, the condition (22) is approximately satisfied in the vicinity of the following values of P_Ω [see dashed black rectangles in Fig. 4(a)]:

$$P_\Omega = \{4.2; 6.5; 8.1; 9.8; 11.4; 13.1; 14.6; \dots\}. \quad (23)$$

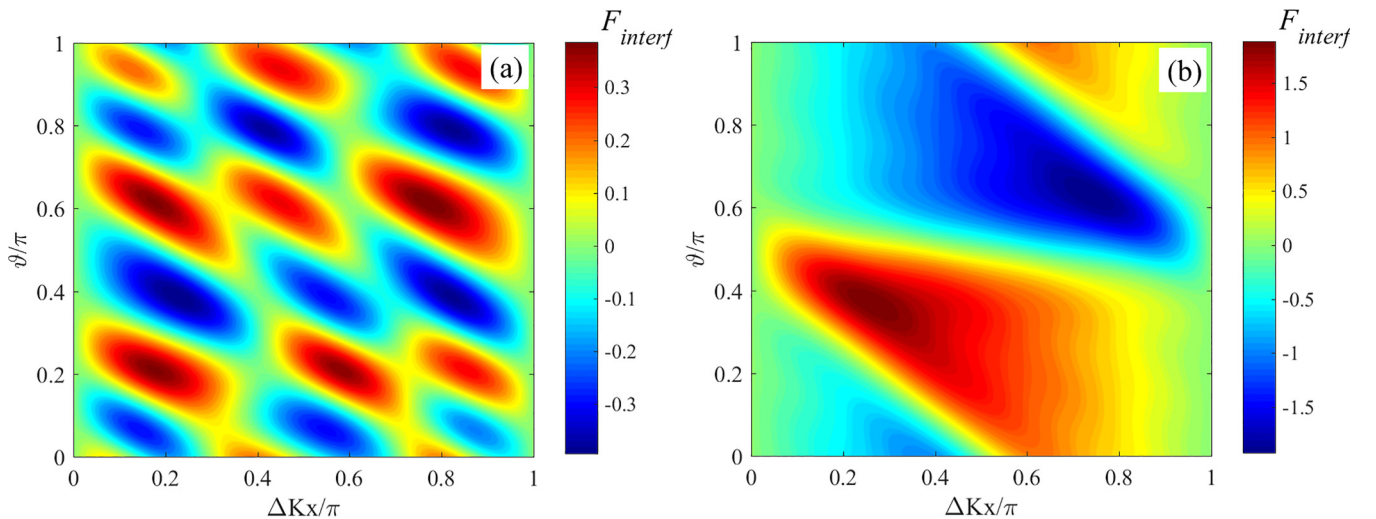


FIG. 5. The dependence of F_{interf} on the normalized propagation distance, ΔKx , and the initial phase of the modulating field, ϑ , for (a) the first group [blue circles in Fig. 4(b)] and (b) the second group [red stars in Fig. 4(b)] of the modulation indices, P_Ω .

As in the case of three harmonics, the modulation indices (23) are divided into two groups. The first group includes $P_\Omega = \{4.2; 8.1; 11.4; 14.6; \dots\}$ [blue circles in Fig. 4(b)], for which $J_0(P_\Omega) \simeq -J_2(P_\Omega) \simeq -J_4(P_\Omega)$. The corresponding dependence $F_{\text{interf}}^{(1)}(\Delta Kx, \vartheta)$ is shown in Fig. 5(a). In this case, the areas of the positive contribution of the coherently scattered field to the total field (5), $F_{\text{interf}} > 0$ (and thus $G_{\text{coh}} > 0$), are small, while the peak value of $F_{\text{interf}}^{(1)}$ is $\max\{F_{\text{interf}}^{(1)}\} \simeq 0.38$, which is smaller than in Fig. 3. The reduction in the peak value of $F_{\text{interf}}^{(1)}$ is caused by low synchronization between the different components of the coherently scattered field. Thus, for the modulation indices from the first group, the effect of MAHH for five in-phase harmonics is relatively weak and unstable with respect to variation of ΔKx and ϑ .

The second group of the modulation indices includes $P_\Omega = \{6.5; 9.8; 13.1; \dots\}$ [red stars in Fig. 4(b)], for which $J_0(P_\Omega) \simeq -J_2(P_\Omega) \simeq J_4(P_\Omega)$. For these modulation indices the dependence $F_{\text{interf}}^{(2)}(\Delta Kx, \vartheta)$ is shown in Fig. 5(b). In contrast with Fig. 5(a), for the modulation indices from the second group the effect of MAHH is stronger and more stable with respect to variation of the parameters ΔKx and ϑ , since, in this case, $\max\{F_{\text{interf}}^{(2)}\} \simeq 1.92 > \max\{F_{\text{interf}}^{(1)}\}$, while the range of $F_{\text{interf}} > 0$ is wider. Moreover, qualitatively Fig. 5(b) resembles Fig. 3(b). The peak value of $F_{\text{interf}}^{(2)}$ is reached at $\Delta Kx \simeq 0.26\pi + p\pi$, where $p = \{0, 1, 2, \dots\}$, and $\vartheta \simeq 0.37\pi$. Under these conditions, as for a set of three HHs, we have $\Delta Kx + 2\vartheta = \pi + p\pi$ and $\text{sgn}(J_{2m}J_{2n}) = (-1)^{m-n}$. Thus, according to Eq. (14), in this case all components of the coherently scattered field are in phase with each other and with amplified harmonics, except for the contribution from the -2 th harmonic to the field of the $+2$ th harmonic, which is approximately zero.

Now we formulate the optimal conditions for MAHH for a set of five HHs, which maximize the factors $J^2(P_\Omega)$ and F_{interf} . According to Fig. 4(b), the peak value of J^2 is reached at $P_\Omega = 4.2$ from the first group of the modulation indices; in this case, $J^2(4.2) \simeq 0.10$. However, in this case the peak value of F_{interf} is rather small, $\max\{F_{\text{interf}}^{(1)}\} \simeq 0.38$, and the corresponding value of G_{coh} normalized to the factor $2\alpha f(g_{\text{eff}x}, \gamma_z \tau)$ is about

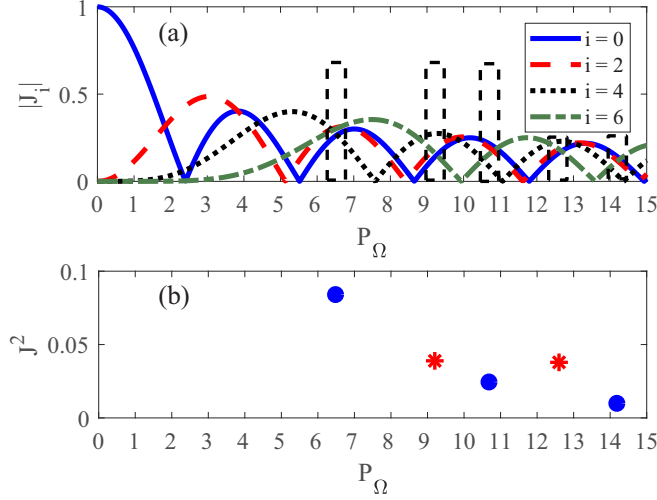


FIG. 6. (a) The modulation index dependence of the absolute value of the i th Bessel function. Blue solid, red dashed, black dotted, and green dash-dotted curves correspond to $i = 0, 2, 4, 6$, respectively. Dashed black rectangles show the ranges of P_Ω , where the condition (24) is approximately satisfied. (b) The square of the averaged absolute values of Bessel functions of orders $i = -6, -4, -2, 0, 2, 4, 6$, $J^2(P_\Omega)$, for the modulation indices satisfying the condition (24). Blue circles correspond to the first group of P_Ω , for which $J_0(P_\Omega) \approx -J_2(P_\Omega) \approx J_4(P_\Omega) \approx J_6(P_\Omega)$, and red stars correspond to the second group of P_Ω , for which $J_0(P_\Omega) \approx -J_2(P_\Omega) \approx -J_4(P_\Omega) \approx -J_6(P_\Omega)$.

0.04; therefore, the effect of MAHH is relatively weak. On the other hand, due to the highest normalized effective gain factors of the harmonics, $g_{mn} \sim J^2$, the value $P_\Omega = 4.2$ is ideal for the independent amplification of five in-phase HHs in a highly dispersive plasma medium [45]. At the same time, for the second group of the modulation indices the peak value of J^2 is reached at $P_\Omega = 6.5$ and corresponds to $J^2(6.5) \simeq 0.081$, while $\max\{F_{\text{interf}}^{(2)}\} \simeq 1.92$. In this case, the normalized value of G_{coh} is about 0.16, which is four times larger than in the case of $P_\Omega = 4.2$. Thus, the optimal conditions for mutual amplification of five in-phase HHs are $P_\Omega \equiv P_\Omega^{(5\text{Harm})} \simeq 6.5$, $\Delta Kx \equiv (\Delta Kx)_{5\text{Harm}} \simeq 0.26\pi + p\pi$, $p = \{0, 1, 2, \dots\}$, and $\vartheta \equiv \vartheta_{5\text{Harm}} \simeq 0.37\pi$.

C. Mutual amplification of seven in-phase HHs

In the case of amplification of a set of seven in-phase HHs, the condition of uniform harmonic amplification has the form

$$|J_0(P_\Omega)| \simeq |J_2(P_\Omega)| \simeq |J_4(P_\Omega)| \simeq |J_6(P_\Omega)|. \quad (24)$$

The modulation index intervals, within which the condition (24) is approximately satisfied, are shown in Fig. 6(a) by dashed black rectangles. They are centered around the following values of P_Ω :

$$P_\Omega = \{6.5; 9.2; 10.7; 12.6; 14.2; \dots\}. \quad (25)$$

The corresponding square of the averaged absolute value of Bessel functions of even orders from -6 th to 6 th, $J^2(P_\Omega)$, is shown in Fig. 6(b). As in the previous cases, the modulation indices (25) can be divided into two groups.

The first group includes the modulation indices $P_\Omega = \{6.5; 10.7; 14.2; \dots\}$ [blue circles in Fig. 6(b)]. For these val-

ues of the modulation index $J_0(P_\Omega) \simeq -J_2(P_\Omega) \simeq J_4(P_\Omega) \simeq J_6(P_\Omega)$. The first two of these equalities are the same as in the optimal case for mutual amplification of a set of five HHs. Moreover, the modulation indices from the first group are close to the optimal ones for the amplification of five HHs, while the dependence $F_{\text{interf}}^{(1)}(\Delta Kx, \vartheta)$ shown in Fig. 7(a) resembles Fig. 5(b). However, adding the two harmonics to the incident field [with the gain coefficients proportional to $J_6^2(P_\Omega)$] makes the dependence $F_{\text{interf}}^{(1)}(\Delta Kx, \vartheta)$ somewhat spotty and reduces the peak value of the parameter F_{interf} in comparison with the case of five harmonics from 1.923 to 0.787. This is due to the fact that for the considered modulation indices the sign of $J_6(P_\Omega)$ is the same as that of $J_0(P_\Omega)$ and $J_4(P_\Omega)$. As a result, the total coherently scattered field includes the components [the terms in the sum in (14) or (18)] which are in antiphase with the incident HH field. In particular, for $\Delta Kx \simeq 0.36\pi + p\pi$, where $p = \{0, 1, 2, \dots\}$, and $\vartheta \simeq 0.32\pi$, at which $F_{\text{interf}}^{(1)}(\Delta Kx, \vartheta)$ reaches its maximum value, 10 out of 36 components of the coherently scattered field are out of phase [ten terms in (18) are negative], while under the optimal conditions of mutual amplification of five HHs, all components of the coherently scattered field are in phase with the incident harmonics. Thus, the first group of the modulation indices is not optimal for MAHH. On the other hand, the modulation index $P_\Omega = 6.5$ corresponds to the largest normalized gain factor, J^2 , and thus is optimal for the independent amplification of seven HHs [44,45].

The second group of the modulation indices includes the values $P_\Omega = \{9.2; 12.6; \dots\}$ [red stars in Fig. 6(b)], for which $J_0(P_\Omega) \simeq -J_2(P_\Omega) \simeq J_4(P_\Omega) \simeq -J_6(P_\Omega)$. In contrast to the modulation indices from the first group, in this case the sign of $J_6(P_\Omega)$ is opposite to the sign of $J_0(P_\Omega)$. Thus, $\text{sgn}(J_{2n}J_{2m}) = (-1)^{m-n}$ as in the optimal cases for mutual amplification of three and five HHs. This causes the similarity of the dependence $F_{\text{interf}}^{(2)}(\Delta Kx, \vartheta)$ shown in Fig. 7(b) to the dependencies plotted in Figs. 3(b) and 5(b). In the considered case, the peak value $\max\{F_{\text{interf}}^{(2)}\} \simeq 2.15$ is reached at $\Delta Kx \simeq 0.2\pi + p\pi$, where $p = \{0, 1, 2, \dots\}$, and $\vartheta \simeq 0.4\pi$. For these values of the parameters ΔKx and ϑ all components of the coherently scattered field, except for two, which are generated due to scattering from the -3 rd to the $+3$ rd HH and vice versa, are in phase with the field of harmonics. For the modulation indices from the second group, the maximum value of $J^2 \simeq 0.039$ is reached at $P_\Omega = 9.2$, see Fig. 6(b), and corresponds to the value of $G_{\text{coh}}/2\alpha f(g_{\text{eff}x}, \gamma_z \tau)$ of about 0.08. Thus, the optimal conditions for mutual amplification of the set of seven in-phase harmonics are $P_\Omega \equiv P_\Omega^{(7\text{Harm})} \simeq 9.2$, $\Delta Kx \equiv (\Delta Kx)_{7\text{Harm}} \simeq 0.2\pi + p\pi$, where $p = \{0, 1, 2, \dots\}$, and $\vartheta \equiv \vartheta_{7\text{Harm}} \simeq 0.4\pi$.

In the next section, for the found optimal values of the parameters, we numerically study the MAHH effect using the active medium of an x-ray laser based on a Li^{2+} hydrogenlike plasma as an example. The obtained results are compared with the case of independent harmonic amplification in a plasma medium with high free-electron concentration.

IV. NUMERICAL RESULTS

Below we present numerical calculations, which are based on the integration of the set of Maxwell-Bloch equations, for

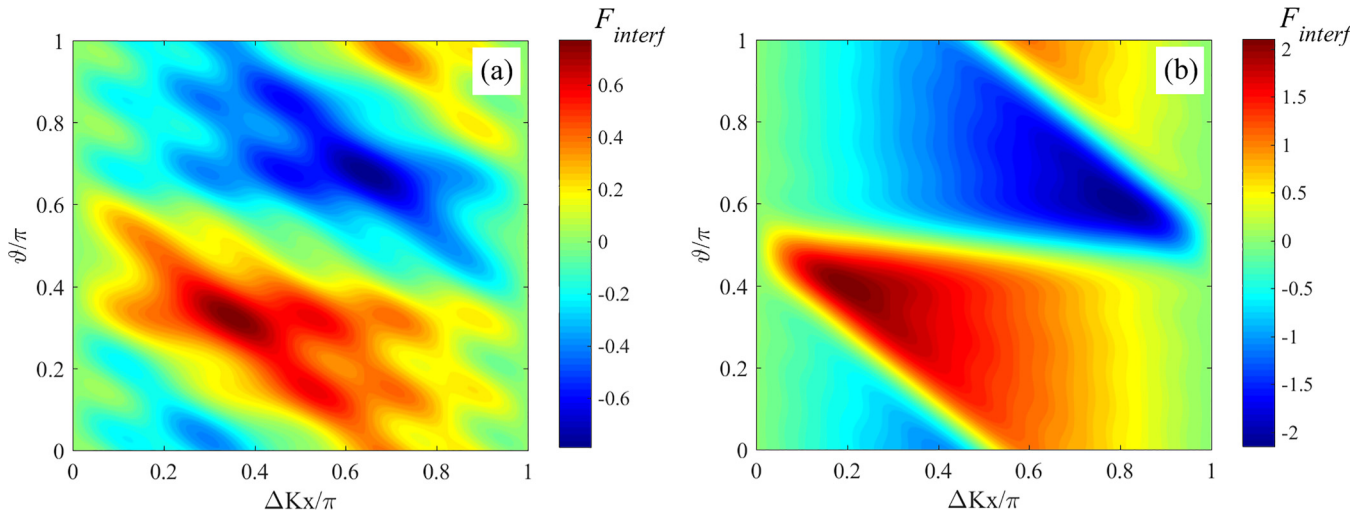


FIG. 7. The dependence of F_{interf} on the normalized propagation distance, ΔKx , and the initial phase of the modulating field, ϑ , for (a) the first group [blue circles in Fig. 6(b)] and (b) the second group [red stars in Fig. 6(b)] of the modulation indices, P_{Ω} .

detailed consideration of the possibilities of mutual amplification of HHs (3) in a moderately dispersive active medium of an x-ray laser based on a hydrogenlike Li^{2+} plasma. In contrast to the analytical solution presented above, this approach does not rely on the perturbation theory when taking into account mutual harmonic scattering, and also takes into account (i) the change in the population differences at the inverted transitions, as well as (ii) amplified spontaneous emission generated at the transitions $|4\rangle \leftrightarrow |1\rangle$ and $|5\rangle \leftrightarrow |1\rangle$; this emission can overlap in time and space with amplified harmonic radiation and lead to a decrease in the harmonic amplification efficiency due to an increase in the population of the ground state of the ions. Both factors are taken into account in a five-level model of the active medium described in detail in [44,47,48]. This model takes into account all dipole-allowed transitions between the considered bound states. In the general case, it would also be necessary to take into account a decrease in the population of the excited states due to their single-photon ionization by the high-harmonic radiation (3) resonant to the transition $n = 1 \leftrightarrow n = 2$, resulting in a decrease in harmonic amplification efficiency. However, the probability of the corresponding bound-free transitions is much lower than that of the considered bound-bound transitions, since the squares of the moduli of the dipole moments of bound-free transitions are several tens of times smaller than those of the bound-bound transitions. In particular, the square of the modulus of the dipole moment of single-photon transitions from the excited states $|2\rangle$ and $|3\rangle$ to the continuum states is about 50 times smaller than the square of the modulus of the dipole moment of the transitions from the same states to the ground state $|1\rangle$, which makes it possible to neglect the influence of single-photon ionization in the process of HH amplification.

In the following, we consider the hydrogenlike active medium of a Li^{2+} plasma-based x-ray laser with the inverted transition wavelength in the vicinity of 13.5 nm. We assume the Li^{2+} ion density $N_{\text{ion}} = 1.5 \times 10^{17} \text{ cm}^{-3}$ and the ion temperature 1 eV, as well as the concentration of free electrons $N_e = 3 \times 10^{17} \text{ cm}^{-3}$ with the electron temperature of 2 eV.

These parameters are the same as in [47,48] and close to those in the experiment [52]. The collisional and radiative decay rates of the quantum coherences at the inverted transitions in such a plasma medium are $\gamma_{\text{coll}}^{-1} \approx 0.425 \text{ ps}$ and $\Gamma_{\text{rad}}^{-1} \approx 19.7 \text{ ps}$, respectively. Here, the collisional decay rate is estimated according to [55] in the quasistatic approximation and is determined by ion-ion collisions (the effect of electron-ion collisions for the considered parameter values is negligible). Similarly to the previous works [44,47,48], we assume that initially (before the arrival of resonant radiation at a given point of the medium) all Li^{2+} ions are excited with equal probability to one of the states $|2\rangle$, $|3\rangle$, $|4\rangle$, and $|5\rangle$, while the ground state $|1\rangle$ is not populated. Thus, the initial value of the population inversion between each of the excited states and the ground state is $1/4$, $n_{\text{tr}} = 0.25$. Below we consider an active plasma medium of a cylindrical shape with a cross-sectional radius of $2.5 \mu\text{m}$ and a length of up to 3 mm.

For comparison with analytical results, in numerical calculations we assume a rectangular envelope of the field of each harmonic from the incident set of $(2N + 1)$ HHs (3) with smoothed turn-on and turn-off:

$$E_{\text{in}}(t) = E_0 \times \begin{cases} \sin^2\left(\frac{\pi}{2} \frac{t}{\Delta t_{\text{sw}}}\right), & 0 \leq t < \Delta t_{\text{sw}}, \\ 1, & \Delta t_{\text{sw}} \leq t < \Delta t_{\text{flat}} + \Delta t_{\text{sw}}, \\ \cos^2\left(\frac{\pi}{2} \frac{t - (\Delta t_{\text{flat}} + \Delta t_{\text{sw}})}{\Delta t_{\text{sw}}}\right), & \Delta t_{\text{flat}} + \Delta t_{\text{sw}} \leq t < \Delta t_{\text{flat}} + 2\Delta t_{\text{sw}}, \\ 0, & t \geq \Delta t_{\text{flat}} + 2\Delta t_{\text{sw}}, \end{cases} \quad (26)$$

where $\Delta t_{\text{sw}} = 10 \text{ fs}$ and $\Delta t_{\text{flat}} = 2980 \text{ fs}$. The incident field is nonzero within the time interval $\Delta t_{\text{flat}} + 2\Delta t_{\text{sw}} = 3 \text{ ps}$, has a constant amplitude E_0 within $\Delta t_{\text{flat}} = 2980 \text{ fs}$, and is turned on and off within $\Delta t_{\text{sw}} = 10 \text{ fs}$. The amplitude E_0 is chosen so that the peak intensity of HHs was 10^9 W/cm^2 regardless of the number of harmonics (for an arbitrary N). In turn, the intensity of the modulating field is $I_L = 4 \times 10^{14} \text{ W/cm}^2$, which is close to its maximum allowable value determined by the ionization threshold from the upper lasing states of the ions. Since $P_{\Omega} \sim E_L \Lambda$, for a fixed value of the modulation index, maximization of intensity of the modulating

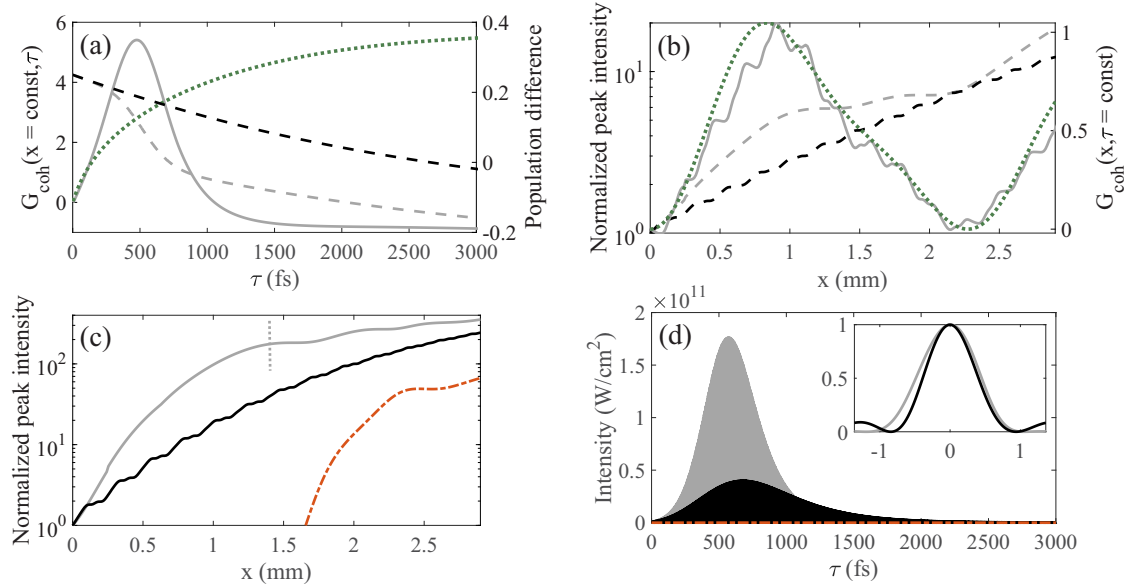


FIG. 8. The results of calculations for a set of three in-phase high-order harmonics. The parameter values are as follows: $P_{\Omega}^{(3\text{Harm})} = 3.83$, $I_L = 4 \times 10^{14} \text{ W/cm}^2$, $\Lambda = 1.63 \text{ }\mu\text{m}$, $\vartheta_{3\text{harm}} = 0.31\pi$, $N_{\text{ion}} = 1.5 \times 10^{17} \text{ cm}^{-3}$, and the electron concentration is either $N_e = 3 \times 10^{17} \text{ cm}^{-3}$ or $3 \times 10^{18} \text{ cm}^{-3}$. For all the figures gray and brown (dash-dotted) curves correspond to the numerical simulations for $N_e = 3 \times 10^{17} \text{ cm}^{-3}$, black curves correspond to the numerical simulations for $N_e = 3 \times 10^{18} \text{ cm}^{-3}$, and green dotted curves correspond to the analytical solution (17)–(19) for $N_e = 3 \times 10^{17} \text{ cm}^{-3}$. (a) The time dependences of G_{coh} (gray solid and green dotted curves, left vertical axis) and of the (common) population difference at the transitions $|2\rangle \rightarrow |1\rangle$ and $|3\rangle \rightarrow |1\rangle$, n_{tr} (gray and black dashed curves, right vertical axis), at the medium length $x = 0.87 \text{ mm}$. (b) The spatial dependences of the peak intensity of an individual z -polarized subfemtosecond pulse produced in the closest vicinity of $\tau = 100 \text{ fs}$, normalized to the peak intensity of the incident pulses, $I_0 = 10^9 \text{ W/cm}^2$ (gray and black dashed curves, left vertical axis), and of the parameter G_{coh} (gray solid and green dotted curves, right vertical axis) at the time instant $\tau = 100 \text{ fs}$. (c) The spatial dependences of the peak intensities (the global maxima throughout the envelope) of the z -polarized pulse train (gray and black solid curves) and of the y -polarized ASE (brown dash-dotted curve), normalized to I_0 . In this panel, each point of each curve corresponds to the different time instant τ , when the maximum of XUV intensity at the corresponding propagation distance is reached. (d) The time dependences of the z -polarized subfemtosecond pulse train (gray and black solid curves) and of the y -polarized ASE (brown dash-dotted curve) at the medium length $x = 1.4 \text{ mm}$ [the corresponding point is marked in (c) by a short dotted gray line]. The inset in (d) shows the pulse shapes at the maxima of the envelope of the corresponding pulse trains.

field (and, thus, its amplitude, E_L) minimizes the modulating wavelength, Λ . A decrease in Λ results in a weaker plasma dispersion for the modulating field (smaller ΔK) and, as a consequence, a larger parameter $\alpha = g_0/\Delta K$ (8), which maximizes the efficiency of mutual harmonic scattering. For the considered intensity of the modulating field, the rate of tunnel ionization from the states $|2\rangle$ and $|3\rangle$ is $\Gamma_{\text{ion}}^{-1} = 3.3 \text{ ps}$. Taking into account all relaxation processes, the characteristic lifetime of coherences at the transitions $|2\rangle \rightarrow |1\rangle$ and $|3\rangle \rightarrow |1\rangle$ is $\gamma_z^{-1} \approx 395 \text{ fs}$. For numerical simulation of the process of independent amplification of high harmonics in a strongly dispersive plasma medium, we increase the electron concentration tenfold, to $N_e = 3 \times 10^{18} \text{ cm}^{-3}$, assuming the presence of a nonresonant impurity in the plasma. As shown below, this concentration is sufficient to suppress the effect of MAHH.

Let us start with the MAHH for a set of three in-phase HHs. In this case, the optimal value of the modulation index is $P_{\Omega}^{(3\text{Harm})} = 3.83$. For the modulating intensity $I_L = 4 \times 10^{14} \text{ W/cm}^2$ it corresponds to the modulating field wavelength $\Lambda = 1.63 \text{ }\mu\text{m}$. First of all, let us consider the results of analytical (17)–(19) and numerical solutions for the time dependences of G_{coh} shown in Fig. 8(a) by green dotted and gray

solid curves, respectively (left vertical axis). The calculations were carried out for the analytically obtained optimum values of the medium length, $x = 0.87 \text{ mm}$ [which corresponds to $(\Delta K x)_{3\text{Harm}} \approx 0.38\pi + p\pi$ at $p = 0$], and the initial phase of the modulating field, $\vartheta_{3\text{Harm}} \approx 0.31\pi$. At the initial moments of time, a good agreement is observed between these curves. However, for the considered parameter values, the sufficient condition (13) for the applicability of the analytical solution (17)–(19) is not satisfied, since $\alpha(\ln N + 1)/(2N + 1) \approx 3.6$. The agreement between the analytical and numerical results at the initial instants of time is due to the finite response time of the resonant medium. At the very beginning of the amplification process, the amplitude of each harmonic due to its self-amplification grows with time faster than the amplitudes of the coherently scattered fields from other harmonics. This, in particular, is reflected in the presence of the factor $(1 - i\omega/\gamma_z)^{-1}$ under the sum symbol in the analytical expressions (6) and (7) for the spectral amplitude of the harmonic field. For this reason, at the initial moments of time, the independent amplification of high harmonics is stronger than the mutual harmonic scattering, which is a necessary condition for the applicability of the analytical solution. In the case of amplification of three HHs, agreement is observed up to the time values $\tau = 120 \text{ fs}$. At longer times, up to 470 fs, G_{coh}

grows faster than the analytical solution (17)–(19) predicts. This is due to the fact that the mutual harmonic scattering becomes comparable to or even stronger than the harmonic self-scattering, so that MAHH starts to dominate in the amplification process, and the analytical solution (17)–(19) based on the perturbation theory becomes incorrect. It can be shown that in the limit of zero plasma dispersion for the modulating field, that is, for $\Delta K \rightarrow 0$ and $\alpha \rightarrow \infty$, under the optimal conditions of MAHHs the harmonics form a “strongly amplified mode,” which grows as a whole with the gain factor given by the sum of the effective gain coefficients for all harmonics from the seeding field (3). This strongly amplified mode is just the same as the “strongly absorbing mode” found for the IR-field-dressed hydrogenlike resonantly absorbing medium in the limit $\Delta K \rightarrow 0$ [56], except for the opposite sign of the population differences at the resonant atomic transitions. The case shown in Fig. 8 is intermediate between the formation of the strongly amplified mode and the predictions of the analytical solution (17)–(19) due to the weak but not vanishing plasma dispersion at the frequency of the modulating field. As a result, at the corresponding moments of time, $120 \leq \tau \leq 470$ fs, the peak intensity of the pulses produced by the total harmonic field, taking into account the mutual harmonic scattering, is higher than predicted by the analytical solution (17)–(19). At the considered radiation intensity of the seed (3), the amplified HH pulse train becomes so intense that its leading edge takes all the energy stored in the population inversion of the active medium, which leads to a shortening of the amplified signal envelope. At even longer times, a decline in G_{coh} is observed, which corresponds to a decrease in the difference $I_{\text{pulse}} - I_{\text{pulse}}^{(\text{indep})}$. This is because, in the case of MAHH, the population difference n_{tr} becomes negative at these times [Fig. 8(a), right vertical axis, gray dashed curve], and the HH radiation is absorbed. At the same time, in the case of independent amplification of harmonics, the population difference is positive [Fig. 8(a), right vertical axis, black dashed curve], and thus the HH radiation is amplified. At a certain instant in time, the pulses in the case of mutual amplification become less intense than in the case of independent amplification, and G_{coh} becomes negative.

Next, we consider the spatial dependence of G_{coh} shown in Fig. 8(b) (right vertical axis) for a time instant of 100 fs. It can be seen that the analytical solution (green dotted curve) agrees well with the results of numerical calculation (gray solid curve). Both the spatial period of G_{coh} and the positions of its maxima are well reproduced and, for the considered values of the modulating field wavelength, $\Lambda = 1.63 \mu\text{m}$, and free-electron concentration, $N_e = 3 \times 10^{17} \text{ cm}^{-3}$, correspond to $L_p = \pi/\Delta K \approx 2.3 \text{ mm}$ and $x_{3\text{Harm}} \approx 0.87 \text{ mm} + pL_p$ [which follows from $(\Delta K x)_{3\text{Harm}} \simeq 0.38\pi + p\pi$], respectively. In Fig. 8(b) (left vertical axis) we also show the spatial dependences of the peak intensity of the single pulse from the pulse train, whose moment of formation is closest to 100 fs, in the case of MAHH, I_{pulse} (gray dashed curve), and the independent harmonic amplification, $I_{\text{pulse}}^{(\text{indep})}$ (black dashed curve). It is interesting to note that the maxima of the spatial dependence of $G_{\text{coh}}(x)$ are reached at those thicknesses of the medium where the spatial dependence of the peak pulse intensity in the case of MAHH, $I_{\text{pulse}}(x)$, reaches saturation. In addition, at the considered time $\tau = 100$ fs, $I_{\text{pulse}} \geq I_{\text{pulse}}^{(\text{indep})}$ at any depth of the

active medium, which confirms the optimal choice of the initial phase of the modulating field, $\vartheta_{3\text{Harm}}$, since otherwise, in accordance with Fig. 3, for certain thicknesses of the medium, the inverse inequality $I_{\text{pulse}} < I_{\text{pulse}}^{(\text{indep})}$ would hold. It is also worth noting the small-scale periodic structure, observed in the numerically calculated spatial dependence of G_{coh} [see Fig. 8(b), right vertical axis, gray solid curve]. This is primarily due to residual (strongly suppressed but nonzero) mutual harmonic scattering in a plasma with high free-electron concentration (in the case of $N_e = 3 \times 10^{18} \text{ cm}^{-3}$), which leads to small-scale oscillations in spatial dependencies of both $I_{\text{pulse}}^{(\text{indep})}(x)$ and $G_{\text{coh}}(x)$, with the period $L_p^{(\text{dense})} \approx 0.23 \text{ mm}$. With an increase in the free-electron concentration, the amplitude and period of these oscillations are reduced, and the numerically calculated dependence $G_{\text{coh}}(x)$ becomes closer to its analytical counterpart.

Of greater practical importance is the spatial dependence of the peak intensity of a pulse train formed by a set of in-phase HHs. It characterizes the ultimate capabilities of harmonic amplification in the considered medium, which, apart from the finite amplification bandwidth, are limited by the nonlinearity of the medium and, in general, ASE. The corresponding dependence in the case of mutual amplification of a set of three in-phase harmonics is shown in Fig. 8(c) by the gray solid curve. It consists of two regions. In the first one, due to MAHH, the peak intensity of the pulse train grows faster than in the case of independent harmonic amplification [black solid curve in Fig. 8(c)]. The medium length, at which the greatest difference in the peak intensities is observed, is about 1 mm, which is close to the analytically obtained value, 0.87 mm. In the second region, the growth of the peak intensity of the pulse train in the case of MAHHs reaches saturation and proceeds slowly compared to the independent harmonic amplification. The gain slowdown in an active medium with low free-electron concentration is caused by a decrease in the amplitude of the coherently scattered field [as in the gray dashed curve in Fig. 8(b)] and depletion of the population inversion at resonant transitions $|2\rangle \rightarrow |1\rangle$ and $|3\rangle \rightarrow |1\rangle$ by the HH radiation, whose intensity in this case exceeds the saturation threshold. From a practical point of view, it is reasonable to use an active medium with a thickness corresponding to the transition between these two regions (where the saturation intensity is reached by the HH field). According to Fig. 8(c), for the considered values of the parameters, such a transition occurs near 1.4 mm [it is marked in Fig. 8(c) with a short dotted gray line]. It is also worth noting that at all considered thicknesses of the active medium, ASE of y polarization [Fig. 8(c), brown dash-dotted curve] is significantly less intensive compared to the radiation of the amplified HHs.

In Fig. 8(d) we also show the time dependences of the intensity of a set of three in-phase HHs in the cases of their mutual and independent amplification ($N_e = 3 \times 10^{17} \text{ cm}^{-3}$, gray curve, and $N_e = 3 \times 10^{18} \text{ cm}^{-3}$, black curve, respectively) at the medium thickness of 1.4 mm [marked in Fig. 8(c) with a short dotted gray line]. As can be seen, due to the presence of a coherently scattered field and its synchronization with the HH radiation, in the case of MAHHs the intensity of the amplified pulses is considerably higher (except for the

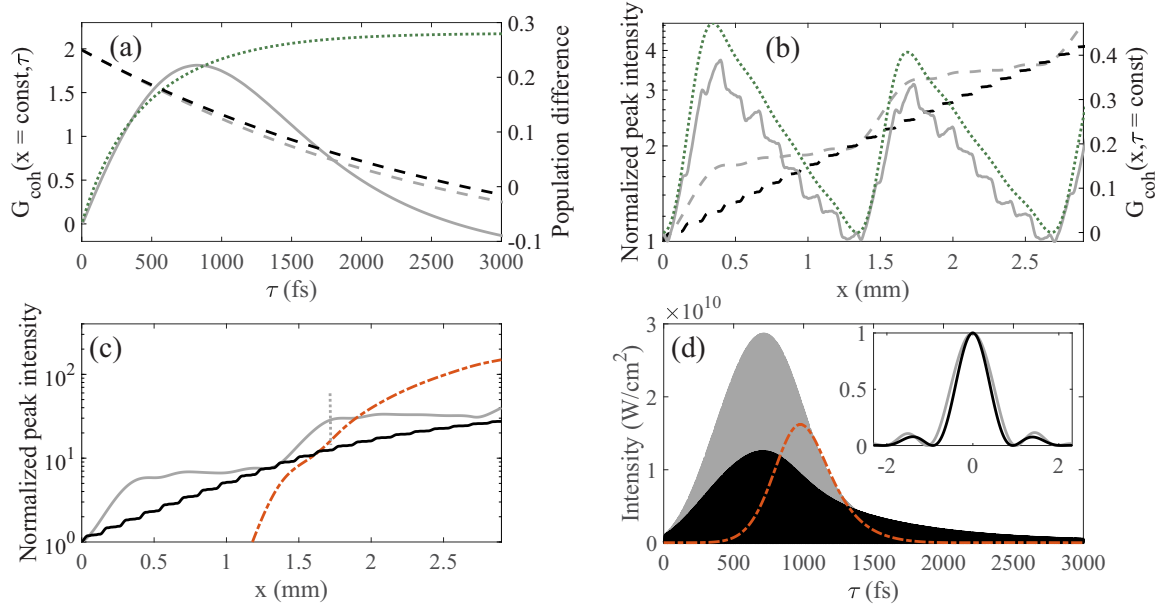


FIG. 9. Same as in Fig. 8, but for a set of five in-phase high-order harmonics. The parameter values are as follows: $P_{\Omega}^{(5\text{Harm})} = 6.5$, $I_L = 4 \times 10^{14} \text{ W}/\text{cm}^2$, $\Lambda = 2.77 \mu\text{m}$, $N_{\text{ion}} = 1.5 \times 10^{17} \text{ cm}^{-3}$, $\vartheta_{5\text{harm}} = 0.37\pi$, and the electron concentration is either $N_e = 3 \times 10^{17} \text{ cm}^{-3}$ or $3 \times 10^{18} \text{ cm}^{-3}$. Panel (a) corresponds to the medium thickness $x = 0.35 \text{ mm}$, panel (b) is plotted for $\tau = 100 \text{ fs}$, while panel (d) is plotted for $x = 1.72 \text{ mm}$ [the latter value is marked in panel (c) by a short dotted gray line].

trailing edge of the pulse sequence, for which the medium becomes absorbing). In particular, the peak intensity of the pulse train reaches $1.8 \times 10^{11} \text{ W}/\text{cm}^2$, which is about 4.4 times greater than in the case of independent harmonic amplification. As shown in the inset in Fig. 8(d), the shape of individual pulses in both cases remains nearly the same, while their full width at half maximum (FWHM) is slightly (1.18 times) larger in a plasma with low free-electron concentration.

Next, we similarly consider the mutual amplification of five in-phase HHs. In this case, the optimal value of the modulation index is $P_{\Omega}^{(5\text{Harm})} = 6.5$. At the modulating intensity $I_L = 4 \times 10^{14} \text{ W}/\text{cm}^2$ the corresponding wavelength of the modulating field is $\Lambda = 2.77 \mu\text{m}$. In Fig. 9 we show the dependences similar to those shown in Fig. 8. The regularities described above for a set of three in-phase high-order harmonics are also valid for the case of five HHs. Therefore, consider the differences between Figs. 9 and 8. First, because of longer wavelength of the modulating field and, as a consequence, stronger plasma dispersion at its frequency, the coherently scattered field in the case of five HHs is weaker than for a set of three harmonics. As a result, analytical solution (17)–(19) is valid over a longer time interval, at least up to about 450 fs [see Fig. 9(a)]. However, at the initial moments of time, the analytical solution slightly overestimates the value of G_{coh} [see Fig. 9(b) plotted for $\tau = 100 \text{ fs}$]. This is due to the fact that, in contrast to the case of three HHs, where the gain coefficients of all harmonics under optimal conditions are exactly the same [see (20)], for the case of five HHs there is a small spread in both the gain coefficients and the cross products of the Bessel functions of different orders, which characterize the amplitudes of the mutually scattered fields [see Fig. 4(a) for $P_{\Omega} = 6.5$]. In addition, due to larger value of the modulation index, the effective gain for a set of five HHs is approximately

two times lower than for three harmonics, which leads to a lower intensity of the amplified signal at the same propagation distance. As a result, the saturation intensity is not reached, and the decay of the population difference at the resonant transitions $|2\rangle \rightarrow |1\rangle$ and $|3\rangle \rightarrow |1\rangle$ in Fig. 9(a) both for plasmas with low and high free-electron concentrations (see gray and black dashed curves, respectively) occurs mainly due to spontaneous transitions. Hereupon, the spatial dependence of the peak intensity of the pulse train [the global maximum over the local time τ , gray solid curve in Fig. 9(c)] qualitatively reproduces the spatial dependence of the peak intensity of a single pulse in the immediate vicinity of $\tau = 100 \text{ fs}$ [which corresponds to the initial stage of the amplification process and is shown by the gray dashed curve in Fig. 9(b)]. The lower gain of HHs also enhances the role of y-polarized ASE [see Fig. 9(c)]. Thus, according to Fig. 9(c), the amplified harmonic radiation dominates over the y-polarized ASE only up to a medium thickness of 1.9 mm. In Fig. 9(d) we plot the time dependence of the intensity of a set of five HHs in the case of their mutual amplification (gray solid curve) for a slightly thinner medium 1.72 mm thick [which corresponds to a short dotted gray line in Fig. 9(c)], where the transition occurs between the regions of the fastest and slowest rise in the peak intensity of the pulse train. For comparison, the same time dependence is shown in the case of independent harmonic amplification (black solid curve), as well as the time dependence of the intensity of the y-polarized ASE (brown dash-dotted curve). As can be seen, due to the synchronized coherently scattered field, the peak intensity of the pulse train increases by about 2.3 times, while the shape of the pulses is maintained with a slight (by about 1.19 times) increase in the duration of each of the pulses compared to the case of independent harmonic amplification.

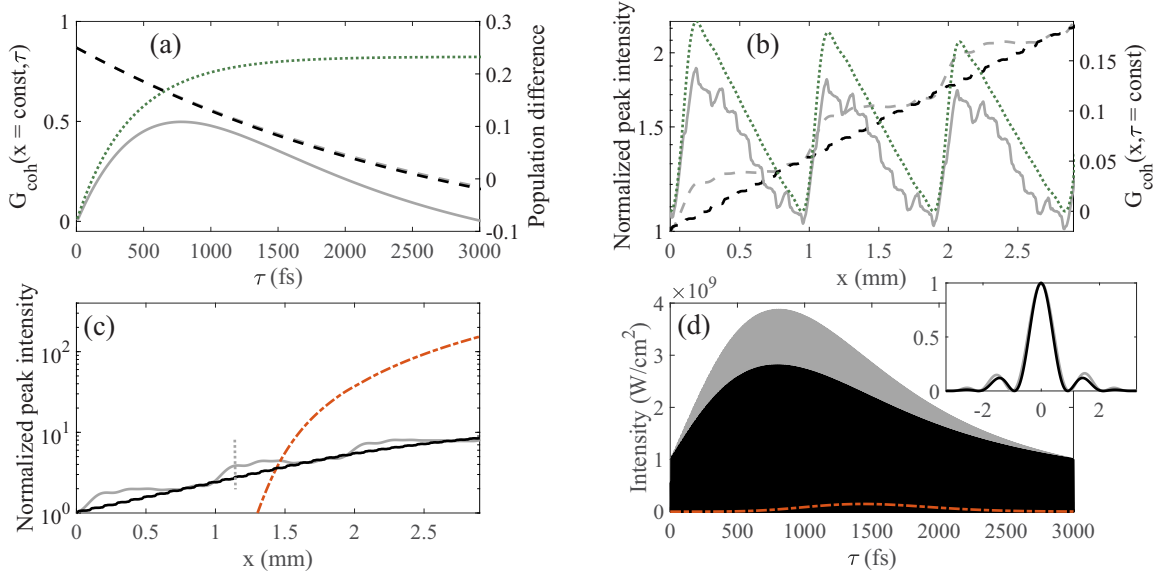


FIG. 10. Same as in Figs. 8 and 9, but for a set of seven in-phase high-order harmonics. The parameter values are as follows: $P_{\Omega}^{(7\text{Harm})} = 9.2$, $I_L = 4 \times 10^{14}$ W/cm², $\Lambda = 3.92$ μm , $N_{\text{ion}} = 1.5 \times 10^{17}$ cm⁻³, $\vartheta_{7\text{harm}} = 0.4\pi$, and the electron concentration is either $N_e = 3 \times 10^{17}$ cm⁻³ or 3×10^{18} cm⁻³. Panel (a) corresponds to the medium thickness $x = 0.19$ mm, panel (b) corresponds to $\tau = 100$ fs, while panel (d) corresponds to $x = 1.14$ mm [which is marked in panel (c) with the short dotted gray line].

Finally, we consider the case of mutual amplification of seven in-phase HHs. In this case, at the intensity of the modulating field $I_L = 4 \times 10^{14}$ W/cm², the optimal value of the modulation index $P_{\Omega}^{(7\text{Harm})} = 9.2$ is reached for the modulating field with a wavelength $\Lambda = 3.92$ μm . The main features of the mutual amplification of a set of seven in-phase HHs are illustrated in Fig. 10 and are similar to the cases of three (Fig. 8) and five (Fig. 9) HHs. However, due to the even longer wavelength of the modulating field, which results in a higher modulation index and lower effective gain for each of the harmonics, the effect of MAHH and the overall amplification of the harmonics are even weaker than in the case of amplification of five HHs. Moreover, due to the greater spread in the harmonic gain values, the analytical solution overestimates G_{coh} even more compared to the results of numerical calculations [Figs. 10(a) and 10(b)]. The range of medium lengths, at which the y-polarized ASE is less intense than the HH radiation, also decreases [Fig. 10(c)]. We chose 1.14 mm [marked by a short dotted gray line in Fig. 10(c)] as the medium length, where the MAHH effect is comparably strong, while the peak intensity of HH pulses is high and the y-polarized ASE is negligible. According to Fig. 10(d), synchronization of the coherently scattered field with a set of seven in-phase HHs makes it possible to increase the peak intensity of the pulse train by a factor of 1.4 without changing the shape of the corresponding pulses compared to the case of independent harmonic amplification.

So far, we have considered the case when the harmonics of different orders, forming a train of subfemtosecond pulses, have the same amplitudes. However, in reality, even in the plateau region the amplitudes of neighboring harmonics produced via the HHG in a gas can differ significantly, for example, due to the interference of the contributions of different trajectories of the recombining electron [57,58]. The difference in the amplitudes of the seed HHs leads both (i) to

a change in the shape of the pulses incident to the medium and (ii) to a change in the amplitudes of the spectral components of the multifrequency coherently scattered field (caused by the dependence of the efficiency of HH scattering into each other on the amplitudes of the scattered harmonics). This can result in a change in the shape and duration of the pulses at the exit from the modulated active medium.

As an example, we consider the case of mutual amplification of a set of five HHs. In order not to specify the dependence of harmonic amplitudes on their orders, we consider a random equiprobable distribution of the amplitude of an individual harmonic with a 40% spread both up and down around the average value. In this case, the average value of the harmonic amplitude is the same as in the case of equal amplitudes of the five HHs and the pulse intensity of 10^9 W/cm² (as in Fig. 9). Figure 11(a) shows the amplitude spectrum of one of the random realizations of the amplitude distribution of HHs, while the corresponding pulse shape is shown in Fig. 11(b) by the black dotted curve. For comparison, Figs. 11(c) and 11(d) show similar dependences for the case of equal harmonic amplitudes. Despite the spread in the amplitudes of the harmonics, the pulse shape and duration at the entrance to the medium change insignificantly except for the more pronounced pulse pedestal in Fig. 11(b) in comparison with Fig. 11(d). It is noteworthy that the found optimal conditions for mutual amplification of five HHs with equal amplitudes, i.e., the intensity, wavelength, and initial phase of the modulating field, as well as the thickness of the medium, remain optimal for the case of nonuniform distribution of HH amplitudes as long as the seed HHs are in phase with each other. In Figs. 11(b) and 11(d) we also show the corresponding pulse shapes at the exit from the modulated active medium under the optimal conditions (blue solid curves). In both cases, the shape of the pulses is practically unchanged; moreover, the pulse FWHM increases by approximately the

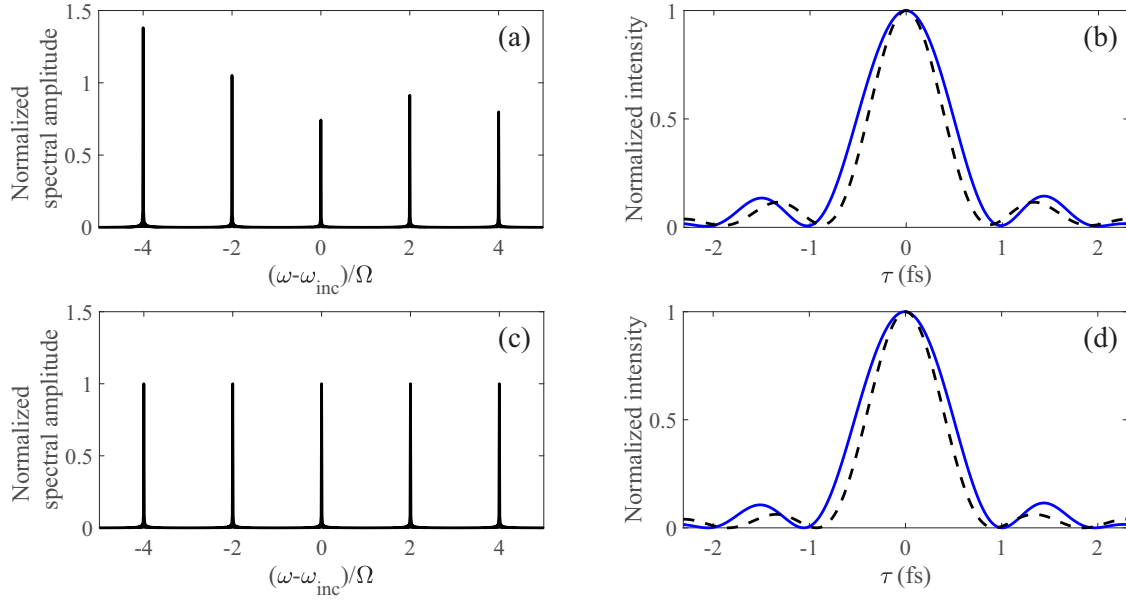


FIG. 11. Amplitude spectra for a set of five in-phase HHs at the entrance to the medium (a), (c), as well as the pulse shapes near the maxima of the envelopes of the corresponding pulse trains (b), (d) at the entrance to (black dashed curves) and exit from (blue solid curves) the medium. Panels (a) and (b) correspond to a random amplitude distribution under a 40% uniform spread of HH amplitudes (both below and above), the average value corresponding to the HH amplitude in panel (c). Panels (c) and (d) correspond to the case of equal HH amplitudes. The parameter values are the same as in Fig. 9. In panels (b) and (d) blue solid curves are plotted for $x = 1.72$ mm. The normalization coefficients for spectral amplitudes in (a) and (c) are the same.

same factor 1.2. Thus, MAHH is robust with respect to a change in the distribution of HH amplitudes at the entrance to the medium.

V. CONCLUSION

In the present paper, we investigated the possibility of amplifying a set of in-phase high-order harmonics, forming a train of subfemtosecond pulses, in a hydrogenlike active medium of a plasma-based x-ray laser with low free-electron concentration, which is additionally irradiated by a strong laser field of the fundamental frequency (a replica of the field used to generate harmonics). In contrast to the active medium with high free-electron concentration [44], in this case, modulation by the laser field leads not only to the amplification of HHs, but also to their mutual coherent scattering into each other. The efficiency of this scattering essentially depends on the difference in phase velocities between the modulating field and the field of HHs: the larger it is, the proportionally smaller is the amplitude of the coherently scattered field. It is shown that synchronization of a coherently scattered field with the radiation of the amplified HHs results in their constructive interference leading to the increase in the intensity of the total output radiation by several times. We call this effect the mutual amplification of high-order harmonics.

We derived an analytical solution considering the mutual harmonic scattering as a perturbation and used it to optimize the conditions of MAHH for a set of a given number of in-phase HHs, under which (i) the maximum increase in the intensity of the amplified pulses of high harmonics in the case of their mutual amplification compared to the case of independent harmonic amplification (in a medium with a high

free-electron concentration) is reached and (ii) the shape of the amplified pulses is preserved. These optimal conditions correspond to such values of intensity, wavelength, and initial phase of the modulating field, as well as thickness of the medium, at which (i) the gain coefficients for harmonics of different orders are close to each other and are the maximum possible and (ii) all spectral components of the coherently scattered field are in phase with the HH field. In this case, the amplification of a set of a larger number of harmonics requires larger intensity and/or wavelength of the modulating field. However, the allowable laser intensity is limited by the ionization threshold of the active medium, while an increase in the wavelength results in stronger plasma dispersion for the modulating field, which reduces the role of MAHH. For this reason, the largest gain in intensity of the amplified pulses due to synchronization of the coherently scattered field is reached for a set of the least number of high harmonics.

The possibilities for the experimental implementation of the discussed effect were considered by the example of an active medium of hydrogenlike Li^{2+} ions with the inverted transition wavelength of 13.5 nm. In this case, the optimal value of the modulating field intensity is 4×10^{14} W/cm², while the corresponding laser wavelengths for a set of three, five, and seven HHs are 1.63, 2.77, and 3.92 μm , respectively.

We also performed numerical calculations based on the Maxwell-Bloch equations in their general form (without using the perturbation theory). These calculations confirm the predictions of the obtained analytical solution concerning, in particular, the location and spatial period of the sections of the medium, where the greatest gain from the mutual amplification of HHs is observed in comparison with the case of their independent amplification. The effect of MAHH is strongest

for a set of three in-phase HHs. In this case, the peak intensity of pulses in the amplified pulse train reaches the saturation value of 1.8×10^{11} W/cm² (at which further intensification of the HH field is limited by the nonlinearity) at a medium thickness of 1.4 mm. This intensity is 4.4 times higher than in the case of independent amplification of high harmonics (in the latter case, the same value of the peak intensity is achieved for a medium with a thickness of 3 mm).

The results obtained open up the possibility of increasing the efficiency of amplification of high harmonics, as well as relaxing the requirements for the parameters of the active medium of a plasma-based x-ray laser. Enhanced spectral

combs and trains of attosecond XUV and x-ray radiation pulses can be used in x-ray spectroscopy, as well as in attosecond metrology and chronoscopy.

ACKNOWLEDGMENTS

I.R.Kh., V.A.A., and M.Yu.R. acknowledge the support of the Center of Excellence ‘‘Center of Photonics’’ funded by the Ministry of Science and Higher Education of the Russian Federation, Grant No. 075-15-2022-316. O.K. appreciates the support of the National Science Foundation (Grant No. PHY-2012194).

APPENDIX A: DERIVATION OF THE EQUATIONS FOR THE SPECTRAL AMPLITUDES OF HARMONICS

Let us consider the system of Eqs. (4) (see main text of the paper):

$$\begin{aligned}\frac{\partial \tilde{E}_z}{\partial x} &= i \frac{4\pi\omega_z N_{\text{ion}} d_{\text{tr}}}{c\sqrt{\epsilon_{\text{XUV}}}} (\tilde{\rho}_{21} - \tilde{\rho}_{31}), \\ \frac{\partial \tilde{\rho}_{21}}{\partial \tau} &= [-\gamma_z + i\Delta_\Omega \cos(\Omega\tau + \Delta Kx + \vartheta)] \tilde{\rho}_{21} - i \frac{d_{\text{tr}} n_{\text{tr}}}{2\hbar} \tilde{E}_z, \\ \frac{\partial \tilde{\rho}_{31}}{\partial \tau} &= [-\gamma_z - i\Delta_\Omega \cos(\Omega\tau + \Delta Kx + \vartheta)] \tilde{\rho}_{31} + i \frac{d_{\text{tr}} n_{\text{tr}}}{2\hbar} \tilde{E}_z.\end{aligned}\quad (\text{A1})$$

We will look for a solution for \tilde{E}_z in the form

$$\tilde{E}_z(x, \tau) = \int_{-\infty}^{\infty} \tilde{A}(x, \omega) e^{-i\omega\tau} d\omega, \quad (\text{A2})$$

where $\tilde{A}(x, \omega)$ is the amplitude of the spectral component at the frequency ω at the propagation distance x inside the medium. Further, let us consider the second equation of the system (A1) and look for its solution in the form

$$\tilde{\rho}_{21}(x, \tau) = \hat{\rho}_{21}(x, \tau) \exp[iP_\Omega \sin(\Omega\tau + \Delta Kx + \vartheta)], \quad (\text{A3})$$

where $P_\Omega = \Delta_\Omega/\Omega$ is the modulation index, and $\hat{\rho}_{21}(x, \tau)$ satisfies the equation

$$\frac{\partial \hat{\rho}_{21}}{\partial \tau} + \gamma_z \hat{\rho}_{21} = -i \frac{d_{\text{tr}} n_{\text{tr}}}{2\hbar} \sum_{k=-\infty}^{\infty} J_k(P_\Omega) e^{-ik(\Delta Kx + \vartheta)} \int_{-\infty}^{\infty} \tilde{A}(x, \omega - k\Omega) e^{-i\omega\tau} d\omega, \quad (\text{A4})$$

which is obtained taking into account (A2) and the equality $e^{iP_\Omega \sin(x)} = \sum_{k=-\infty}^{\infty} J_k(P_\Omega) e^{ikx}$, where $J_k(x)$ is the Bessel function of the first kind of order k . Then we represent $\hat{\rho}_{21}$ in the form of a Fourier integral $\hat{\rho}_{21} = \int_{-\infty}^{\infty} \hat{\rho}_{21}^{(\omega)}(x, \omega) e^{-i\omega\tau} d\omega$, and after substituting it into (A4) get an expression for the spectral amplitude $\hat{\rho}_{21}^{(\omega)}(x, \omega)$:

$$\hat{\rho}_{21}^{(\omega)}(x, \omega) = -i \frac{d_{\text{tr}} n_{\text{tr}}}{2\hbar\gamma_z} \sum_{k=-\infty}^{\infty} J_k(P_\Omega) e^{-ik(\Delta Kx + \vartheta)} \frac{\tilde{A}(x, \omega - k\Omega)}{1 - i\omega/\gamma_z}. \quad (\text{A5})$$

Performing the inverse Fourier transform of (A5) and using (A3), we obtain the following solution for the coherence $\tilde{\rho}_{21}(x, \tau)$:

$$\tilde{\rho}_{21}(x, \tau) = -i \frac{d_{\text{tr}} n_{\text{tr}}}{2\hbar\gamma_z} \sum_{k,m=-\infty}^{\infty} J_k(P_\Omega) J_m(P_\Omega) e^{i(m-k)(\Delta Kx + \vartheta)} \int_{-\infty}^{\infty} \frac{\tilde{A}(x, \omega + (m-k)\Omega)}{1 - i(\omega + m\Omega)/\gamma_z} e^{-i\omega\tau} d\omega. \quad (\text{A6})$$

Similarly, we obtain a solution to the third equation of the system (A1):

$$\tilde{\rho}_{31}(x, \tau) = i \frac{d_{\text{tr}} n_{\text{tr}}}{2\hbar\gamma_z} \sum_{k,m=-\infty}^{\infty} (-1)^{m-k} J_k(P_\Omega) J_m(P_\Omega) e^{i(m-k)(\Delta Kx + \vartheta)} \int_{-\infty}^{\infty} \frac{\tilde{A}(x, \omega + (m-k)\Omega)}{1 - i(\omega + m\Omega)/\gamma_z} e^{-i\omega\tau} d\omega. \quad (\text{A7})$$

Substituting (A6) and (A7) into the first equation of the system (A1) and performing some transformations, we obtain an equation for the spectral amplitude $\tilde{A}(x, \omega)$:

$$\frac{\partial \tilde{A}(x, \omega)}{\partial x} = \sum_{k=-\infty}^{\infty} \frac{g_0 J_k^2(P_\Omega)}{1 - i(\omega + k\Omega)/\gamma_z} \tilde{A}(x, \omega) + \sum_{\substack{k,p=-\infty \\ p \neq 0}}^{\infty} \frac{g_0 J_k(P_\Omega) J_{2p+k}(P_\Omega) e^{i2p(\Delta Kx + \vartheta)}}{1 - i[\omega + (2p+k)\Omega]/\gamma_z} \tilde{A}(x, \omega + 2p\Omega). \quad (\text{A8})$$

Next, we represent the spectrum $\tilde{A}(x, \omega)$ in the form of a set of $2N + 1$ high-order harmonics, which are separated from each other by the frequency interval 2Ω :

$$\tilde{A}(x, \omega) = \sum_{n=-N}^N \tilde{A}_n(x, \omega - 2n\Omega). \quad (\text{A9})$$

Substituting (A9) into (A8), we get the equation for the spectral amplitude of the n th harmonic:

$$\frac{\partial \tilde{A}_n(x, \omega)}{\partial x} = \sum_{k=-\infty}^{\infty} \frac{g_0 J_k^2(P_\Omega)}{1 - i[\omega + (2n + k)\Omega]/\gamma_z} \tilde{A}_n(x, \omega) + \sum_{\substack{k, p=-\infty \\ p \neq 0}}^{\infty} \frac{g_0 J_k(P_\Omega) J_{2p+k}(P_\Omega) e^{i2p(\Delta Kx + \vartheta)}}{1 - i[\omega + (2p + 2n + k)\Omega]/\gamma_z} \tilde{A}_{n+p}(x, \omega), \quad (\text{A10})$$

where we take into account that $\tilde{A}_{n+p}(x, \omega) = \tilde{A}_n(x, \omega + 2p\Omega)$ and $n = -N, -N + 1, \dots, N$. Thus, (A10) is a system of $2N + 1$ equations. Further, we assume that the frequency separation between the harmonics, 2Ω , is much larger than both (i) the spectral linewidth of each high harmonic (so that, in the spectral domain, the neighboring harmonics do not overlap with each other) and (ii) the gain spectrum width of the active medium, $\Omega \gg \gamma_z$. Thus, in (A10) all terms in the sums can be neglected, except for one term in the first sum, corresponding to $k = -2n$, and one term in the second sum, corresponding to $k = -2p - 2n$. We also assume that no new sidebands appear in the spectrum of high harmonics during the amplification process. Thus, in (A10) in the sum over the index p , only the terms with $p = -N - n, -N - n + 1, \dots, N - n$ should be taken into account. After making the substitution $m = n + p$, Eq. (A10) can be rewritten as

$$\frac{\partial \tilde{A}_n(x, \omega)}{\partial x} = \frac{g_0 J_{2n}^2(P_\Omega)}{1 - i\omega/\gamma_z} \tilde{A}_n(x, \omega) + \sum_{\substack{m=-N \\ m \neq n}}^N \frac{g_0 J_{2m}(P_\Omega) J_{2n}(P_\Omega)}{1 - i\omega/\gamma_z} \tilde{A}_m(x, \omega) e^{i2(m-n)(\Delta Kx + \vartheta)}. \quad (\text{A11})$$

Let us seek a solution for $\tilde{A}_n(x, \omega)$ in the form

$$\tilde{A}_n(x, \omega) = \hat{A}_n(x, \omega) \exp \left[\frac{g_0 J_{2n}^2(P_\Omega)}{1 - i\omega/\gamma_z} x \right], \quad (\text{A12})$$

where $\hat{A}_n(x, \omega)$ satisfies the equation

$$\frac{\partial \hat{A}_n(x, \omega)}{\partial x} = \sum_{\substack{m=-N \\ m \neq n}}^N \frac{g_0 J_{2m}(P_\Omega) J_{2n}(P_\Omega)}{1 - \frac{i\omega}{\gamma_z}} \hat{A}_m(x, \omega) e^{\frac{g_0 x}{1 - \frac{i\omega}{\gamma_z}} (J_{2m}^2(P_\Omega) - J_{2n}^2(P_\Omega))} e^{i2(m-n)(\Delta Kx + \vartheta)}. \quad (\text{A13})$$

Integrating (A13) we obtain

$$\hat{A}_n(x, \omega) = \hat{A}_n(x=0, \omega) + \sum_{\substack{m=-N \\ m \neq n}}^N \frac{g_0 J_{2m}(P_\Omega) J_{2n}(P_\Omega) e^{i2(m-n)\vartheta}}{1 - i\omega/\gamma_z} \int_0^x \hat{A}_m(x', \omega) \exp \left[\frac{g_0 x'}{1 - i\omega/\gamma_z} (J_{2m}^2(P_\Omega) - J_{2n}^2(P_\Omega)) + i2(m-n)\Delta Kx' \right] dx'. \quad (\text{A14})$$

Substituting (A14) into (A12) we obtain the following system of interrelated equations for the spectral amplitudes of the harmonics, $\tilde{A}_n(x, \omega)$:

$$\tilde{A}_n(x, \omega) = \tilde{A}_n(x=0, \omega) e^{g_{nm}x/(1-i\omega/\gamma_z)} + \sum_{\substack{m=-N \\ m \neq n}}^N \frac{g_{nm} e^{i2(m-n)\vartheta}}{1 - i\omega/\gamma_z} \int_0^x \tilde{A}_m(x', \omega) e^{g_{mn}(x-x')/(1-i\omega/\gamma_z) + i2(m-n)\Delta Kx'} dx', \quad (\text{A15})$$

where $\hat{A}_n(x=0, \omega) = \tilde{A}_n(x=0, \omega)$ and $g_{nm} = g_0 J_{2n}(P_\Omega) J_{2m}(P_\Omega)$.

APPENDIX B: CALCULATION OF $\tilde{E}_{\text{indep}}(x, \tau)$

The integral

$$\tilde{E}_{\text{indep}}(x, \tau) = \int_{-\infty}^{\infty} \tilde{A}_0(\omega) \exp[g_{\text{eff}}x/(1 - i\omega/\gamma_z)] e^{-i\omega\tau} d\omega \quad (\text{B1})$$

can be calculated using the response function technique in the time domain. In this case, $\tilde{E}_{\text{indep}}(x, \tau)$ equals to the convolution integral of the incident field, $\tilde{E}_{\text{in}}(\tau) = \int_{-\infty}^{\infty} \tilde{A}_0(\omega) e^{-i\omega\tau} d\omega$, and the response function of the resonant amplifier, $R(\tau)$,

$$\tilde{E}_{\text{indep}}(x, \tau) = \int_{-\infty}^{\infty} \tilde{E}_{\text{in}}(t) R(\tau - t) dt, \quad (\text{B2})$$

where

$$R(\tau) = \frac{1}{2\pi} \int_{-\infty}^{\infty} \exp[g_{\text{eff}}x/(1 - i\omega/\gamma_z)] e^{-i\omega\tau} d\omega = \delta(\tau) + \theta(\tau) e^{-\gamma_z\tau} g_{\text{eff}}x\gamma_z \frac{I_1(2\sqrt{g_{\text{eff}}x\gamma_z\tau})}{\sqrt{g_{\text{eff}}x\gamma_z\tau}}. \quad (\text{B3})$$

Here $\delta(\tau)$ is the Dirac delta function and $I_1(x)$ is the first-order modified Bessel function of the first kind. According to Eq. (3) from Sec. II of the main text, $\tilde{E}_{\text{in}}(\tau) = E_0\theta(\tau)$. In this case, the integral (B2) takes the form

$$\tilde{E}_{\text{indep}}(x, \tau) = \theta(\tau) + \theta(\tau) e^{-\gamma_z\tau} \int_0^\tau e^{\gamma_z t} \frac{I_1(2\sqrt{g_{\text{eff}}x\gamma_z(\tau-t)})}{\sqrt{g_{\text{eff}}x\gamma_z(\tau-t)}} g_{\text{eff}}x\gamma_z dt. \quad (\text{B4})$$

By introducing the change of variable, $\xi = 2\sqrt{g_{\text{eff}}x\gamma_z(\tau-t)}$, in the integral in (B4), we rewrite (B4) in equivalent form

$$\tilde{E}_{\text{indep}}(x, \tau) = \theta(\tau) + \theta(\tau) \int_0^{2\sqrt{g_{\text{eff}}x\gamma_z\tau}} I_1(\xi) \exp[-\xi^2/(4g_{\text{eff}}x)] d\xi. \quad (\text{B5})$$

Since $I_1(\xi) = \sum_{k=0}^{\infty} \frac{1}{k!(k+1)!} (\xi/2)^{2k+1}$, by introducing the notation $\eta = \xi^2/(4g_{\text{eff}}x)$ in the integral in (B5), we get

$$\int_0^{2\sqrt{g_{\text{eff}}x\gamma_z\tau}} I_1(\xi) \exp[-\xi^2/(4g_{\text{eff}}x)] d\xi = \sum_{k=0}^{\infty} \frac{(g_{\text{eff}}x)^{k+1}}{k!(k+1)!} \int_0^{\gamma_z\tau} \eta^k e^{-\eta} d\eta. \quad (\text{B6})$$

The integral in (B6) has the form

$$\int_0^{\gamma_z\tau} \eta^k e^{-\eta} d\eta = k! - k! e^{-\gamma_z\tau} \sum_{m=0}^k \frac{(\gamma_z\tau)^m}{m!} = k! e^{-\gamma_z\tau} \sum_{m=k+1}^{\infty} \frac{(\gamma_z\tau)^m}{m!}, \quad (\text{B7})$$

where the expansion $\exp(\gamma_z\tau) = \sum_{m=0}^{\infty} (\gamma_z\tau)^m/m!$ is used. Thus, $\tilde{E}_{\text{indep}}(x, \tau)$ takes the form

$$\tilde{E}_{\text{indep}}(x, \tau) = \theta(\tau) \left[1 + e^{-\gamma_z\tau} \sum_{k=0}^{\infty} \frac{(g_{\text{eff}}x)^{k+1}}{(k+1)!} \sum_{m=k+1}^{\infty} \frac{(\gamma_z\tau)^m}{m!} \right]. \quad (\text{B8})$$

If $\gamma_z\tau < 1$, then the sum over the index m can be estimated from the first term of this series: $\sum_{m=k+1}^{\infty} (\gamma_z\tau)^m/m! \approx (\gamma_z\tau)^{k+1}/(k+1)!$. Thus, the sum in the second term of (B8) is

$$\sum_{k=0}^{\infty} \frac{(g_{\text{eff}}x)^{k+1}}{(k+1)!} \sum_{m=k+1}^{\infty} \frac{(\gamma_z\tau)^m}{m!} \approx \sum_{k=0}^{\infty} \frac{(g_{\text{eff}}x\gamma_z\tau)^{k+1}}{[(k+1)!]^2} = I_0(2\sqrt{g_{\text{eff}}x\gamma_z\tau}) - 1, \quad (\text{B9})$$

and

$$\tilde{E}_{\text{indep}}(x, \tau) \simeq \theta(\tau) [1 + e^{-\gamma_z\tau} (I_0(2\sqrt{g_{\text{eff}}x\gamma_z\tau}) - 1)]. \quad (\text{B10})$$

-
- [1] P. B. Corkum and F. Krausz, Attosecond science, *Nat. Phys.* **3**, 381 (2007).
- [2] F. Krausz and M. Ivanov, Attosecond physics, *Rev. Mod. Phys.* **81**, 163 (2009).
- [3] L. Gallmann, C. Cirelli, and U. Keller, Attosecond science: Recent highlights and future trends, *Annu. Rev. Phys. Chem.* **63**, 447 (2012).
- [4] F. Calegari, G. Sansone, S. Stagira, C. Vozzi, and M. Nisoli, Advances in attosecond science, *J. Phys. B: At. Mol. Opt. Phys.* **49**, 062001 (2016).
- [5] L. Young, K. Ueda, M. Gühr, P. H. Bucksbaum, M. Simon, S. Mukamel, N. Rohringer, K. C. Prince, C. Masciovecchio, M. Meyer, A. Rudenko, D. Rolles, C. Bostedt, M. Fuchs, D. A. Reis, R. Santra, H. Kapteyn, M. Murnane, H. Ibrahim, F. Légaré, M. Vrakking, M. Isinger, D. Kroon, M. Gisselbrecht, A. L'Huillier, H. J. Wörner, and S. R. Leone, Roadmap of ultrafast x-ray atomic and molecular physics, *J. Phys. B: At. Mol. Opt. Phys.* **51**, 032003 (2018).
- [6] R. Schoenlein, T. Elsaesser, K. Holldack, Z. Huang, H. Kapteyn, M. Murnane, and M. Woerner, Recent advances in ultrafast x-ray sources, *Phil. Trans. R. Soc. A* **377**, 20180384 (2019).
- [7] R. Geneaux, H. J. B. Marroux, A. Guggenmos, D. M. Neumark, and S. R. Leone, Transient absorption spectroscopy using high harmonic generation: A review of ultrafast x-ray dynamics in molecules and solids, *Phil. Trans. R. Soc. A* **377**, 20170463 (2019).
- [8] C. Winterfeldt, C. Spielmann, and G. Gerber, Colloquium: Optimal control of high-harmonic generation, *Rev. Mod. Phys.* **80**, 117 (2008).
- [9] M. C. Kohler, T. Pfeifer, K. Z. Hatsagortsyan, and C. H. Keitel, Frontiers of atomic high-harmonic generation, *Adv. At. Mol. Opt. Phys.* **61**, 159 (2012).
- [10] V. V. Strelkov, V. T. Platonenko, A. F. Sterzhantov, and M. Yu. Ryabikin, Attosecond electromagnetic pulses: Generation, measurement, and application. Generation of high-order

- harmonics of an intense laser field for attosecond pulse production, *Phys. Usp.* **59**, 425 (2016).
- [11] K. Zhao, Q. Zhang, M. Chini, Y. Wu, X. Wang, and Z. Chang, Tailoring a 67 attosecond pulse through advantageous phase-mismatch, *Opt. Lett.* **37**, 3891 (2012).
- [12] J. Li, X. Ren, Y. Yin, K. Zhao, A. Chew, Y. Cheng, E. Cunningham, Y. Wang, S. Hu, Y. Wu, M. Chini, and Z. Chang, 53-attosecond x-ray pulses reach the carbon K-edge, *Nat. Commun.* **8**, 186 (2017).
- [13] T. Gaumnitz, A. Jain, Y. Pertot, M. Huppert, I. Jordan, F. Ardana-Lamas, and H. J. Wörner, Streaking of 43-attosecond soft-x-ray pulses generated by a passively CEP-stable mid-infrared driver, *Opt. Express* **25**, 27506 (2017).
- [14] A. S. Johnson, D. R. Austin, D. A. Wood, C. Brahms, A. Gregory, K. B. Holzner, S. Jarosch, E. W. Larsen, S. Parker, C. S. Strüber, P. Ye, J. W. G. Tisch, and J. P. Marangos, High-flux soft x-ray harmonic generation from ionization-shaped few-cycle laser pulses, *Sci. Adv.* **4**, eaar3761 (2018).
- [15] Y. Fu, K. Nishimura, R. Shao, A. Suda, K. Midorikawa, P. Lan, and E. J. Takahashi, High efficiency ultrafast water-window harmonic generation for single-shot soft x-ray spectroscopy, *Commun. Phys.* **3**, 92 (2020).
- [16] P. Salières, A. L’Huillier, and M. Lewenstein, Coherence Control of High-Order Harmonics, *Phys. Rev. Lett.* **74**, 3776 (1995).
- [17] E. J. Takahashi, P. Lan, O. D. Mücke, Y. Nabekawa, and K. Midorikawa, Attosecond nonlinear optics using gigawatt-scale isolated attosecond pulses, *Nat. Commun.* **4**, 2691 (2013).
- [18] P. Tzallas, E. Skantzakis, L. A. A. Nikolopoulos, G. D. Tsakiris, and D. Charalambidis, Extreme-ultraviolet pump-probe studies of one-femtosecond-scale electron dynamics, *Nat. Phys.* **7**, 781 (2011).
- [19] L. Roos, E. Constant, E. Mevel, P. Balcou, D. Descamps, M. B. Gaarde, A. Valette, R. Haroutunian, and A. L’Huillier, Controlling phase matching of high-order harmonic generation by manipulating the fundamental field, *Phys. Rev. A* **60**, 5010 (1999).
- [20] L. A. Lompre, A. L’Huillier, M. Ferray, P. Monot, G. Mainfray, and C. Manus, High-order harmonic generation in xenon: Intensity and propagation effects, *J. Opt. Soc. Am. B* **7**, 754 (1990).
- [21] S. Kazamias, F. Weihe, D. Douillet, C. Valentin, T. Planchon, S. Sebban, G. Grillon, F. Augé, D. Hulin, and Ph. Balcou, High order harmonic generation optimization with an apertured laser beam, *Eur. Phys. J. D* **21**, 353 (2002).
- [22] C. Jin, A. T. Le, and C. D. Lin, Medium propagation effects in high-order harmonic generation of Ar and N₂, *Phys. Rev. A* **83**, 023411 (2011).
- [23] H. W. Sun, P. C. Huang, Y. H. Tzeng, J. T. Huang, C. D. Lin, C. Jin, and M. C. Chen, Extended phase matching of high harmonic generation by plasma-induced defocusing, *Optica* **4**, 976 (2017).
- [24] C. Jin, M.-C. Chen, H.-W. Sun, and C. D. Lin, Extension of water-window harmonic cutoff by laser defocusing-assisted phase matching, *Opt. Lett.* **43**, 4433 (2018).
- [25] C. Jin, G. Wang, H. Wei, A.-T. Le, and C. D. Lin, Waveforms for optimal sub-keV high-order harmonics with synthesized two- or three-colour laser fields, *Nat. Commun.* **5**, 4003 (2014).
- [26] C. Jin, G. Wang, A.-T. Le, and C. D. Lin, Route to optimal generation of soft x-ray high harmonics with synthesized two-color laser pulses, *Sci. Rep.* **4**, 7067 (2014).
- [27] C. Jin, K.-H. Hong, and C. D. Lin, Optimal generation of high harmonics in the water-window region by synthesizing 800-nm and mid-infrared laser pulses, *Opt. Lett.* **40**, 3754 (2015).
- [28] T. Kroh, C. Jin, P. Krogen, P. D. Keathley, A.-L. Calendron, J. P. Siqueira, H. Liang, E. L. Falcao-Filho, C. D. Lin, F. X. Kartner, and K.-H. Hong, Enhanced high-harmonic generation up to the soft x-ray region driven by mid-infrared pulses mixed with their third harmonic, *Opt. Express* **26**, 16955 (2018).
- [29] X. Li, J. Fan, J. Ma, G. Wang, and C. Jin, Application of optimized waveforms for enhancing high-harmonic yields in a three-color laser-field synthesizer, *Opt. Express* **27**, 841 (2019).
- [30] S. Haessler, T. Balčiunas, G. Fan, G. Andriukaitis, A. Pugžlys, A. Baltuška, T. Witting, R. Squibb, A. Zair, J. W. G. Tisch, J. P. Marangos, and L. Chipperfield, Optimization of Quantum Trajectories Driven by Strong-Field Waveforms, *Phys. Rev. X* **4**, 021028 (2014).
- [31] A. S. Emelina, M. Yu. Emelin, R. A. Ganeev, M. Suzuki, H. Kuroda, and V. V. Strelkov, Two-color high-harmonic generation in plasmas: Efficiency dependence on the generating particle properties, *Opt. Express* **24**, 13971 (2016).
- [32] K. J. Schafer, M. B. Gaarde, A. Heinrich, J. Biegert, and U. Keller, Strong Field Quantum Path Control Using Attosecond Pulse Trains, *Phys. Rev. Lett.* **92**, 023003 (2004).
- [33] M. B. Gaarde, K. J. Schafer, A. Heinrich, J. Biegert, and U. Keller, Large enhancement of macroscopic yield in attosecond pulse train-assisted harmonic generation, *Phys. Rev. A* **72**, 013411 (2005).
- [34] A. Heinrich, W. Kornelis, M. P. Anscombe, C. P. Hauri, P. Schlup, J. Biegert, and U. Keller, Enhanced VUV-assisted high harmonic generation, *J. Phys. B: At. Mol. Opt. Phys.* **39**, S275 (2006).
- [35] E. J. Takahashi, T. Kanai, K. L. Ishikawa, Y. Nabekawa, and K. Midorikawa, Dramatic Enhancement of High-Order Harmonic Generation, *Phys. Rev. Lett.* **99**, 053904 (2007).
- [36] F. Brizuela, C. M. Heyl, P. Rudawski, D. Kroon, L. Rading, J. M. Dahlstrom, J. Mauritsson, P. Johnsson, C. L. Arnold, and A. L’Huillier, Efficient high-order harmonic generation boosted by below-threshold harmonics, *Sci. Rep.* **3**, 1410 (2013).
- [37] B. W. J. McNeil, N. R. Thompson, D. J. Dunning, and B. Sheehy, High harmonic attosecond pulse train amplification in a free electron laser, *J. Phys. B: At. Mol. Opt. Phys.* **44**, 065404 (2011).
- [38] N. R. Thompson and B. W. J. McNeil, Mode Locking in a Free-Electron Laser Amplifier, *Phys. Rev. Lett.* **100**, 203901 (2008).
- [39] P. Zeitoun, G. Faivre, S. Sebban, T. Mocek, A. Hallou, M. Fajardo, D. Aubert, P. Balcou, F. Burgy, D. Douillet, S. Kazamias, G. de Lacheze-Murel, T. Lefrou, S. le Pape, P. Mercere, H. Merdji, A. S. Morlens, J. P. Rousseau, and C. Valentin, A high-intensity highly coherent soft x-ray femtosecond laser seeded by a high harmonic beam, *Nature (London)* **431**, 426 (2004).
- [40] F. Pedaci, Y. Wang, M. Berrill, B. Luther, E. Granados, and J. J. Rocca, Highly coherent injection-seeded 13.2 nm tabletop soft x-ray laser, *Opt. Lett.* **33**, 491 (2008).
- [41] Y. Wang, E. Granados, F. Pedaci, D. Alessi, B. Luther, M. Berrill, and J. J. Rocca, Phase-coherent, injection-seeded, tabletop soft-x-ray lasers at 18.9 nm and 13.9 nm, *Nat. Photon.* **2**, 94 (2008).
- [42] J. A. Koch, B. J. MacGowan, L. B. Da Silva, D. L. Matthews, J. H. Underwood, P. J. Batson, R. W. Lee, R. A. London, and

- S. Mrowka, Experimental and theoretical investigation of neon-like selenium x-ray laser spectral linewidths and their variation with amplification, *Phys. Rev. A* **50**, 1877 (1994).
- [43] O. Guilbaud, F. Tissandier, J.-P. Goddet, M. Ribière, S. Sebban, J. Gautier, D. Joyeux, D. Ros, K. Cassou, S. Kazamias, A. Klisnick, J. Habib, P. Zeitoun, D. Benredjem, T. Mocek, J. Nedjl, S. de Rossi, G. Maynard, B. Cros, A. Boudaa, and A. Calisti, Fourier-limited seeded soft x-ray laser pulse, *Opt. Lett.* **35**, 1326 (2010).
- [44] V. A. Antonov, K. C. Han, T. R. Akhmedzhanov, M. Scully, and O. Kocharovskaya, Attosecond Pulse Amplification in a Plasma-Based x-ray Laser Dressed by an Infrared Laser Field, *Phys. Rev. Lett.* **123**, 243903 (2019).
- [45] I. R. Khairulin, V. A. Antonov, M. Yu. Ryabikin, and O. Kocharovskaya, Enhanced amplification of attosecond pulses in a hydrogen-like plasma-based x-ray laser modulated by an infrared field at the second harmonic of fundamental frequency, *Photonics* **9**, 51 (2022).
- [46] I. R. Khairulin, V. A. Antonov, M. Yu. Ryabikin, M. A. Berrill, V. N. Shlyaptsev, J. J. Rocca, and O. Kocharovskaya, Amplification of elliptically polarized sub-femtosecond pulses in neon-like x-ray laser modulated by an IR field, *Sci. Rep.* **12**, 6204 (2022).
- [47] T. R. Akhmedzhanov, V. A. Antonov, A. Morozov, A. Goltsov, M. Scully, S. Suckewer, and O. Kocharovskaya, Formation and amplification of subfemtosecond x-ray pulses in a plasma medium of hydrogenlike ions with a modulated resonant transition, *Phys. Rev. A* **96**, 033825 (2017).
- [48] I. R. Khairulin, V. A. Antonov, M. Yu. Ryabikin, and O. Kocharovskaya, Sub-fs pulse formation in a seeded hydrogen-like plasma-based x-ray laser dressed by an infrared field: Analytical theory and numerical optimization, *Phys. Rev. Res.* **2**, 023255 (2020).
- [49] V. A. Antonov, I. R. Khairulin, and O. Kocharovskaya, Attosecond-pulse formation in the water-window range by an optically dressed hydrogen-like plasma-based C^{5+} x-ray laser, *Phys. Rev. A* **102**, 063528 (2020).
- [50] I. R. Khairulin, V. A. Antonov, M. Yu. Ryabikin, and O. A. Kocharovskaya, Influence of Detuning of the Seeding VUV Radiation from the Resonance on Formation of Subfemtosecond Pulses in the Active Medium of the Plasma-Based x-ray Laser Dressed by an Intense IR Field, *Phys. Wave Phenom.* **29**, 234 (2021).
- [51] I. R. Khairulin, V. A. Antonov, and O. A. Kocharovskaya, Interference effects in the high-order harmonic amplification process in the active medium of a plasma-based x-ray laser modulated by an optical field, *Quantum Electron.* **50**, 375 (2020).
- [52] D. V. Korobkin, C. H. Nam, S. Suckewer, and A. Goltsov, Demonstration of Soft x-ray Lasing to Ground State in Li III, *Phys. Rev. Lett.* **77**, 5206 (1996).
- [53] Y. Avitzour and S. Suckewer, Feasibility of achieving gain in transition to the ground state of C VI at 3.4 nm, *J. Opt. Soc. Am. B* **24**, 819 (2007).
- [54] T. R. Akhmedzhanov, M. Yu. Emelin, V. A. Antonov, Y. V. Radeonychev, M. Yu. Ryabikin, and O. Kocharovskaya, Ultimate capabilities for few-cycle pulse formation via resonant interaction of XUV radiation with IR-field-dressed atoms, *Phys. Rev. A* **95**, 023845 (2017).
- [55] H. R. Griem, *Spectral Line Broadening by Plasmas* (Academic, New York, 1974).
- [56] I. R. Khairulin, V. A. Antonov, and O. A. Kocharovskaya, Formation of intense attosecond pulses in the sequence of a resonant absorber and active medium of a plasma-based x-ray laser modulated by an optical field, *Radiophys. Quantum Electron.* **64**, 272 (2021).
- [57] A. Zaïr, M. Holler, A. Guandalini, F. Schapper, J. Biegert, L. Gallmann, U. Keller, A. S. Wyatt, A. Monmayrant, I. A. Walmsley, E. Cormier, T. Auguste, J. P. Caumes, and P. Salières, Quantum Path Interferences in High-Order Harmonic Generation, *Phys. Rev. Lett.* **100**, 143902 (2008).
- [58] M. V. Frolov, N. L. Manakov, T. S. Sarantseva, and A. F. Starace, Analytic formulae for high harmonic generation, *J. Phys. B: At. Mol. Opt. Phys.* **42**, 035601 (2009).